



Effect of Green Nanomaterials on CO₂ Diffusion Coefficient and Interfacial Tension in Nanofluids: Implication for CO₂ Sequestrations

Youns T. Youns¹ · Abbas Khaksar Manshad¹

Received: 2 September 2023 / Accepted: 21 November 2023 / Published online: 22 December 2023
© King Fahd University of Petroleum & Minerals 2023

Abstract

This research explores nanomaterials' potential in CO₂ capture and storage, emphasizing their role in CO₂ diffusion and interfacial tension. We aimed to develop eco-friendly nanomaterials and evaluate their impact on CO₂ sequestration, considering factors like pressure, temperature, salinity, and nanoparticle concentration. The research involved experimental measurements of CO₂ diffusion in brine solutions and brine-based nanofluids containing green silica NPs and SiO₂/Xanthan nanocomposites. CO₂ diffusion coefficients were determined through practical pressure decay measurements using the Sheikh method. These measurements were conducted within a Fluid EVAL (PVT) cell, allowing CO₂ interaction with each solution. The results of the study revealed significant improvements in the carbon dioxide (CO₂) diffusion coefficients and reductions in interfacial tension when utilizing water/silica nanofluids containing 0.5 wt.% and 0.1 wt.% concentrations, in comparison with a brine solution without nanoparticles (NPs) and with a high salt concentration (20 wt.% NaCl). The CO₂ diffusion coefficient increased from 2.15E-09 to 4.01E-09 m²/s. An even more significant enhancement was observed with 0.1 wt.% SiO₂ NPs, where the CO₂ diffusion coefficient reached 4.87E-09 m²/s. In addition, CO₂ interfacial tension reduced from 44.3517 to 1.0388 mN/m and 0.9098 mN/m, respectively. The general trend of the measured carbon dioxide diffusion coefficient aligned with increased pressure and temperature. Additionally, when considering the transition to a supercritical state, the findings highlighted consistent behavior, independent of variations in pressure and temperature. Conversely, the interfacial tension between CO₂ and nanofluids decreased in response to heightened pressure and temperature. Moreover, an increase in salinity led to a rise in interfacial tension. In conclusion, heightened CO₂ diffusion and reduced interfacial tension improve CO₂ sequestration, enhancing CO₂ transport, absorption, and storage efficiency for successful long-term CO₂ storage.

Keywords CO₂ sequestration · Nanoparticles · CO₂ diffusion coefficient · CO₂/nanofluid IFT · Governing mechanism

1 Introduction

Global warming and ecological calamities are now caused mainly by anthropogenic greenhouse gas (GHG) emissions [1–3]. Rapid climate change has been cautioned, emphasizing ecosystem dangers and the severe repercussions for human life. According to scientific studies, there is a proven

connection between the rise in atmospheric CO₂ and climate change. In addition, industrial facilities account for the great majority of CO₂ emissions into the atmosphere; the remainder is attributable to automobile emissions and other associated activities [4, 5]. This source is the biggest, with 30% of all CO₂ emissions from power plant flue gas [6, 7]. Various alternative strategies have been used to reduce CO₂ emissions in the atmosphere, including CO₂-free wind and solar energy, geothermal energy, hydrogen generation, and CO₂ geological storage [7, 8].

Carbon dioxide sequestration in geological formations is one effective method to minimize greenhouse gases in the atmosphere [9–12]. This method allows for the disposal of CO₂ by injecting it into deep saline aquifers and depleting oil and gas reserves. Alternatively, it might apply enhanced oil recovery (EOR) techniques to oil reservoirs. Moreover,

✉ Youns T. Youns
yty620h@pete.soran.edu.iq

✉ Abbas Khaksar Manshad
akm113pet@gmail.com

¹ Department of Petroleum Engineering, Faculty of Engineering, Soran University, Soran, Kurdistan Region 44008, Iraq



CO₂ can be injected at the top of a saline aquifer's formation to progressively construct an artificial gas cap above the aquifer [13]. The geological storage technique is crucial in sequestering millions of tons of CO₂ emissions worldwide. With global CO₂ emissions estimated at 36.8 billion tons in 2020 and an increase to 37.5 billion tons by 2022, the need to mitigate the effects of climate change has become even more pressing. To combat climate warming effectively, capturing and securely storing substantial CO₂ emissions within geological formations is imperative. [8].

Immobilizing CO₂ in deep underground rocks is a benefit of CO₂ sequestration, which also helps to create a greener environment. For years, scientists have recognized that sequestering CO₂ in saline aquifers can help mitigate the risks associated with human-caused global warming and reduce global CO₂ emissions. A deep saline sequestration operation's long-term sustainability depends heavily on the amount of CO₂ sequestered and the risk of leakage. However, the low solubility of injected CO₂ in brine remains a problem in contemporary practice, making conventional versions of the process ineffective, expensive, and risky. However, millions of tons of CO₂ are deposited underground every year and, if released into the atmosphere, would increase global warming and lead to irreversible climate change. The interactions between CO₂, brine, and reservoir rock when CO₂ is injected into deep saline aquifers (i.e., at 1071 Psi and 31 °C) have been extensively studied over the past several decades [14]. Based on the research, initially, the injected CO₂ migrates laterally toward the wellbore. Subsequently, the CO₂ gas disperses radially and undergoes dissolution upon reaching the sealing caprock. This dissolution occurs due to the contrasting buoyancies of the CO₂ gas and the in situ interstitial brine, and it precedes interactions with the minerals in the reservoir rock. Due to its tremendous potential, the sequestration of CO₂ using different nanofluids has been offered as a practical solution in the environmental domains. According to Mackay and Gschwend [15], the advanced, original technology of injecting CO₂ with nanofluid in suspension (nano-CO₂) can improve the storage and sequestration of CO₂ in deep saline aquifers. A nanofluid fluid comprises suspended nanoparticles with sizes between 1 and 100 nm (nm) [16]. To create a novel fluid formulation with enhanced thermal, mechanical, or optical properties, the NPs are often distributed in a base fluid like water, oil, or ethylene glycol [17] NPs are now being extensively explored for various subsurface formation applications, notably for CO₂ sequestration.

Measuring carbon dioxide (CO₂) diffusion coefficients is crucial in various fields, including environmental science, chemical engineering, and carbon capture and storage (CCS) research. Accurate determination of CO₂ diffusion coefficients is essential for understanding gas transport in porous media, designing effective CCS strategies, and assessing the

behavior of CO₂ in geological formations [18]. Direct and indirect techniques have been reported in the literature to determine the diffusion coefficient of a gas–liquid binary system. Direct techniques [19]. For example, the capillary cell, Taylor–Aris dispersion, and diaphragm cell are essential for studying gas concentration in liquid samples collected across a range of times. Induced intrusion brought on by sampling and the measuring accuracy of gas concentration is the key issues with direct techniques. Certain indirect techniques were created to alleviate the issues with direct concentration measurements, assessing the changeable features of diffusing gas, such as volume or pressure [20–22]. These techniques include dissolved gas volume and gas pressure decay. The indirect techniques compute the diffusion coefficient and use it to compare the observed characteristic (such as pressure or volume) with a mathematical model to determine the dissolved gas composition in the liquid [23]. Because of its ease of use, accuracy, and simplicity, the pressure decay approach has proven to be one of the most popular ways to measure the diffusion coefficient [24–27] empirically. Direct methods are directly based on Fick's laws and indirect methods. The direct methods consist of steady-state and non-steady-state techniques. Non-steady-state methodologies are founded on Fick's second law for concentration-dependent or concentration-independent diffusivities. Typically, the concentration distribution in a sample is measured, and the diffusion coefficient is derived from a comparison with the appropriate solution of Fick's second law under the experimental conditions. Thin layer methods, diffusion couple methods with and without profile measurement, and in- and out-diffusion are examples of non-steady methods. Not all indirect methods are explicitly based on Fick's laws.

There is a serious lack of data and fundamental knowledge regarding the CO₂ diffusion coefficient and CO₂/nanofluid interfacial tension, which is a crucial parameter determining the risk of leakage, assessing the long-term storage capacity, and determining containment security in the context of CO₂ sequestration (CS), on which we here concentrate. The mass transfer coefficient is increased by adding a small number of solid NPs in the base fluid [28]. According to some studies, the primary mechanism for enhancing the CO₂ diffusion process is the Brownian motion of suspended NPs, comparable to the improvement of heat transmission in nanofluid [29]. Brownian nanoparticle motion and the increase in mass diffusion were examined by Krisnamurthy et al. [30]. They found that compared to deionized water, an Al₂O₃ nanofluid exhibited a higher mass diffusion for the fluorescein dye [30]. Tolesorkhi et al. [31] detected the diffusion of CO₂ into the water and SiO₂ nanofluids at varying nanoparticle concentrations, temperatures, and pressures. They found that adding NPs at lower concentrations (0.1 to 0.5 wt.%) increases Brownian motion, which improves the mass transfer of CO₂ [31]. Other researchers claimed that the Shuttle



Table 1 Summary of the various analytical approaches employed in the literature to measure carbon dioxide (CO₂) diffusion coefficient within the context of NPs [33]

References	Analysis technique	NPs	NPs concentration	Porous media	Operation condition		CO ₂ solubility cm ³ (STP)/cm ³	Diffusion [m ² /s]
					Pres [psi]	Temp [°C]		
Jannatabadi et al. [35]	Solution-diffusion theory	ZIF-8	–	PEGDA/ZIF-8 mixed matrix membranes	58	308	0.15 0.08	2.1×10^{-10} 4.2×10^{-10}
Sharafi et al. [36]	Pressure decay approach	TiO ₂	0 wt.% 3 wt.%	XLPEGDA XLPEGDA/TiO ₂	58	308	1.37 1.63	6.85×10^{-9} 7.98×10^{-9}
Farzami et al. [31]	Pressure decay approach	SiO ₂	0–0.3 wt.%	Water/silica	725.19	308	–	3.48×10^{-9} 2.07×10^{-9}
Zhou et al. [37]	–	PCP filler	–	–	1638.9	321	0.251 0.211	26.6×10^{-8} 54×10^{-8}
Guo et al. [38]	Hidden Intelligent Gravimetric Analyzer	ZIF-8	0 wt.% 17 wt.% 27 wt.%	ZIF-8/P84 MMMs	43.51	298	0.12 0.125 0.14	2.8×10^{-9} 5×10^{-9} 8.5×10^{-9}
Dehghan et al. [39]	Pressure decay approach	– SiO ₂ Al ₂ O ₃ TiO ₂	0 wt.% 0.1 wt.% 0.1 wt.% 0.1 wt.%	–	43.51	35	–	2.25×10^{-10} 8.5×10^{-10} 10.8×10^{-10} 14.7×10^{-10}
Chen et al. [40]	Magnetic suspension balance	CaCO ₃	10 wt.%	PP/nano-CaCO ₃	870–1450	220	0.046 0.04 0.07 0.082	11.8×10^{-10} 10.82×10^{-10} 10^{-10} 12.4×10^{-10} 12.25×10^{-10} 10^{-10}

effect causes the enhancement of mass transfer. The Shuttle effect is a phenomenon that occurs when nanoparticles (NPs) are dispersed throughout a liquid medium. It serves an important function in enhancing mass transfer, which is the movement of molecules between phases. In the context of CO₂ sequestration and nanofluids, the Shuttle effect consists of NPs absorbing gas molecules at the gas–liquid interface and recirculating in the liquid [32]. The recirculation of NPs transporting gas molecules back into the liquid phase results in a mass transfer mechanism that is highly efficient and continuous. This indicates that the captured gas molecules are transported effectively into the liquid phase, resulting in increased dissolution and diffusion rates. Thus, the Shuttle effect increases the overall mass transfer of gases, such as CO₂, into the nanofluid. A summary of the effect of different nanoparticles on CO₂ diffusion coefficient at different conditions of concentration, pressure, and temperatures is shown in Table 1 [33]. It has been demonstrated that NPs significantly affect the CO₂ interfacial tension (IFT) in nanofluids, which helps accelerate CO₂ sequestration processes. CO₂/nanofluid measurements were made under carbon storage conditions by Al-Anssari et al. [34]. They developed new ideas for CO₂ sequestration projects using nanofluids.

This paper conducted several experiments to investigate the impact of green nanomaterials as brine-based NFs on the application of CO₂ sequestration. As a result, this investigation was conducted under the specified circumstances, and experimental measurements of CO₂ gas diffusion and CO₂/nanofluid IFT under various pressure, temperature, concentration, and salinity conditions were made. The pressure decay technique in a Fluid EVAL (PVT) cell and the pendant drop method, respectively, were used to examine the effects of SiO₂ and SiO₂/Xanthan brine-based NFs on CO₂ mass diffusion and CO₂/nanofluid IFT. Additionally, this work established a probable link between diffusion and IFT and the CO₂ sequestration process for the first time.

2 Materials and Methodology

Silicon oxide (SiO₂) green nanoparticles and SiO₂/Xanthan nanocomposites were synthesized in the laboratory, with detailed preparation and synthesis procedures provided in Sect. 2.1. Commercially sourced gas bottles containing 99% pure CO₂ and N₂, along with 2.5 L of toluene and 1 kg of NaCl salt, were utilized. Deionized water of laboratory-grade quality was obtained and employed without further treatment. All chemicals and gases were used in their as-received state.

2.1 Synthesis of SiO₂ and SiO₂/Xanthan NCs

Figure 1 schematically depicts the precise steps of the experimental process for creating SiO₂/Xanthan NCs. The plant extract was initially made by combining 20 gm of dried powdered green leaves with 200 ml of distilled water and stirring for 30 min at a refluxing temperature of 80 °C and 500 rpm. Up to the appearance of black residue, the stirring was continued. The resulting aqueous extract was subsequently filtered and kept at 4 °C. A conical flask containing 250 ml. 200 ml of green leaves extract and 2 g of sodium metasilicate (Na₂SiO₃) were combined in a 250 ml beaker while stirring at 600 rpm at 80 °C. The stirring was kept up until a light black residue was seen to develop. The precipitate was then separated using filtration after being heated in a furnace to 600 °C and washed with hot distillate water to burn and remove all the plant matter and contaminants. After that, 4 gm of xanthan gum was combined with the clean, cool precipitate using a mortar and pestle, and the mixture was refluxed for 5 h at 80 °C. Last, XRD, FSEM, FTIR, and TGA were used to characterize the produced NC.

2.2 Preparation and Characterization of Nanofluid

For measuring their impacts on CO₂ diffusion coefficient in nano-brine-CO₂ systems and IFT reduction, nanofluid with varied concentrations (500, 1000, and 2500 ppm) of SiO₂ NPs and SiO₂/Xanthan NCs were developed and synthesized. The preset weight of the NaCl brine was combined with the prescribed weight of both SiO₂ NPs and SiO₂/Xanthan NCs at various concentrations. Then, the mixture was homogenized using an ultrasonic homogenizer (from Hielscher Company, UP200 model, frequency 20 kHz) for an hour (every 25 min with 5-min rest to prevent overheating). Here, it is essential to emphasize that magnetic stirring is ineffective for creating homogenous nano-suspensions. To carry out this technique, a micro-tip with a diameter of 9.5 mm and energy of 9000 Joules was employed [41].

2.3 Diffusion Coefficient Measurement

In this study, we utilized the versatile Fluid EVAL system provided by Vinci Company for our experimental testing. This testing equipment includes a PVT (Pressure–Volume–Temperature) cell with complete transparency for visual monitoring, an oven for temperature control, and all the essential experimental pipelines. The core component of our experimental setup is the Fluid EVAL PVT cell, as illustrated in Fig. 2. This PVT cell has a comprehensive data acquisition

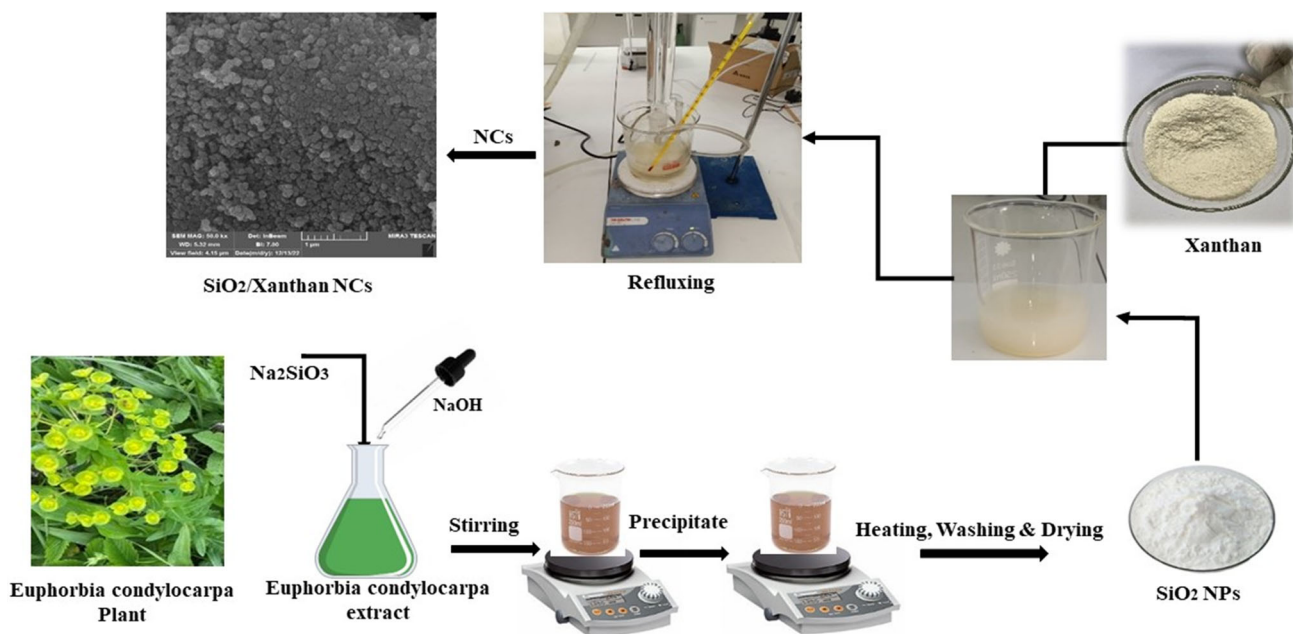


Fig. 1 Schematic of preparing SiO₂ NPs and SiO₂/Xanthan NCs

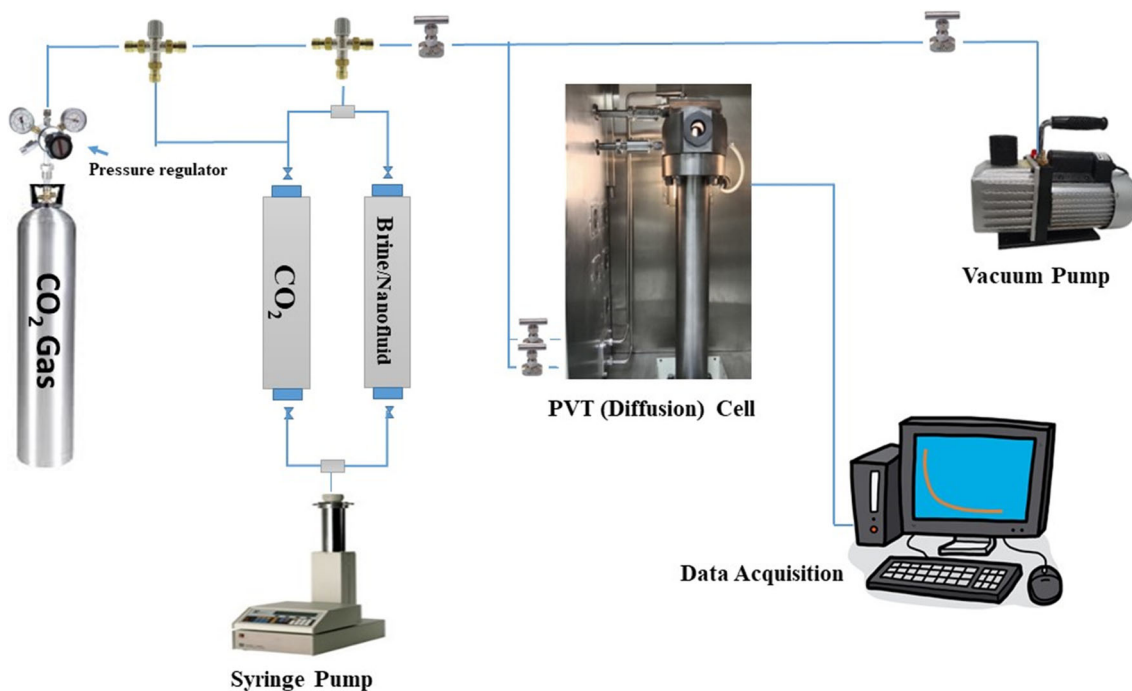


Fig. 2 Schematic of CO₂ diffusion PVT cells (Fluid EVAL)

and processing system, high-pressure valves, interconnected pipelines, a reference pressure transmitter, a reference temperature sensor, and a reliable temperature control system to maintain constant and controlled experimental conditions.

The direct conductivity method is the foundation of the heating system technology. The cell is an HP/HT cylinder

with a maximum capacity of 600 ccs, an internal motorized piston, a 43.7 mm internal diameter, and an outer diameter of 400 mm that enables volume modification. The PVT cylinder operates at 392 °F (200 °C) and 15,000 psi maximum temperature and pressure, respectively.

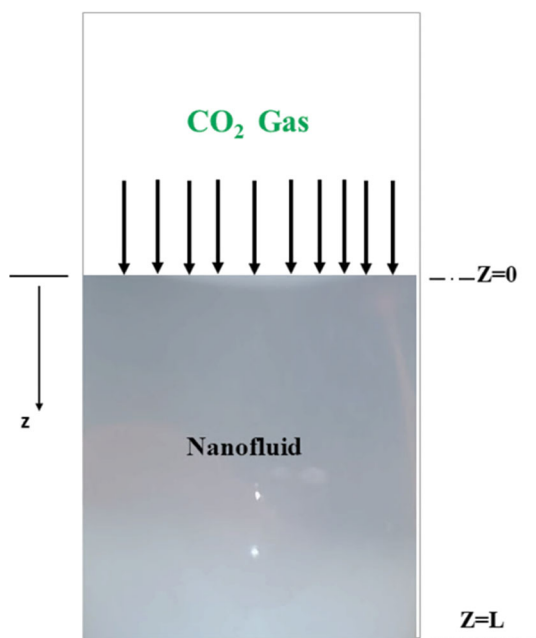


Fig. 3 Schematic of one-dimensional CO₂ diffusion in NF

2.4 Diffusion Coefficient Analytical Calculation

Sheikha et al. [42] obtained an analytical forward solution for that part of a pressure decay experiment predominantly affected by diffusion. Isolation of the corresponding data points using a graphical technique allows the determination of the diffusion coefficient. The analytical solution is obtained by simplifying assumptions, including a non-reactive system, isothermal conditions, constant gas compressibility factor, equilibrium at the gas–fluid interface, and applicability of Henry’s law (Fig. 3).

An infinite-acting model for the estimation of diffusion coefficient can be developed for early times when the diffused gas behaves as if it were diffusing into an infinite cell:

$$C = 0; z \rightarrow \infty, t > 0 \quad (1)$$

[C = concentration of gas in brine (kg/m³), z = depth (m), t = time (s)].

Fick’s second law of diffusion can model the diffusion of gas into the brine:

$$D \frac{\partial^2 C}{\partial z^2} = \frac{\partial C}{\partial t} \quad (2)$$

For the gas-free brine samples used in pressure decay experiments, the initial condition is:

$$C = 0; z \rightarrow \infty, t > 0 \quad (3)$$

The concentration of the gas in the nanofluid can be expressed in terms of pressure by using Henry’s law as follows:

$$P = k_h C \quad (4)$$

[P = pressure (Pa), k_h = Henry’s constant (Pa m³/kg)].

Assuming an equilibrium condition between the gas and nanofluid at a certain pressure, we can express the interface boundary condition as follows:

$$D A \frac{\partial C}{\partial z} \Big|_{z=0} = \frac{VMk_h}{ZRT} \frac{dC}{dt}; z = 0, t > 0 \quad (5)$$

D = diffusion coefficient (m²/s), A = cross-sectional area of the pressure cell (m²), V = volume of gas (m³), M = molar mass of gas (kg/kmol), Z = gas compressibility factor, R = universal gas constant, T = temperature (°C or K).

The mathematical formulation, given by Eqs. (1), (2), (3), and (5), was solved, and the analytical solution in terms of the gas phase (cell) pressure is:

$$P_{(t)} = P_i \cdot \exp\left(\frac{ZRT\sqrt{D}}{LMk_h}\sqrt{t}\right)^2 \operatorname{erfc}\left(\frac{ZRT\sqrt{D}}{LMk_h}\sqrt{t}\right) \quad (6)$$

Sheikha et al. [35] proposed a simplified equation, as shown in (7), for the interpretation of pressure decay data [36].

$$\frac{d\left[\operatorname{erfc}^{-1}\left\{\frac{P(t)}{P_i}\right\}\right]}{d(\sqrt{t})} = \frac{\sqrt{DZRT}}{k_h LM} \quad (7)$$

A graph depicting the complementary $\operatorname{erfc}^{-1}\left\{\frac{P}{P_i}\right\}$ versus \sqrt{t} (Fig. 4) can be utilized to derive the diffusion coefficient plot, which begins with a nonlinear segment, followed by a linear segment. To determine the gas diffusion coefficient in the liquid, you can utilize the slope of the linear segment, as shown in Eq. (8).

$$D = \left(\text{SLOPE} \cdot \frac{LMk_h}{ZRT}\right)^2 \quad (8)$$

2.5 CO₂/Nanofluid IFT Measurement

The pendant drop technique [34] was employed to quantify CO₂/nanofluid γ . The pressure cell was initially heated to the required temperature, and then, CO₂ gas was continually pumped through the cell for 15 min at atmospheric pressure. After closing the output valve, more CO₂ was pumped into the cell using a very accurate syringe pump to increase the pressure to the desired level. The nanofluid was delivered

Fig. 4 The experiment’s $\text{erfc-1 } P(t)/P_i$ profile as a function of root time squared

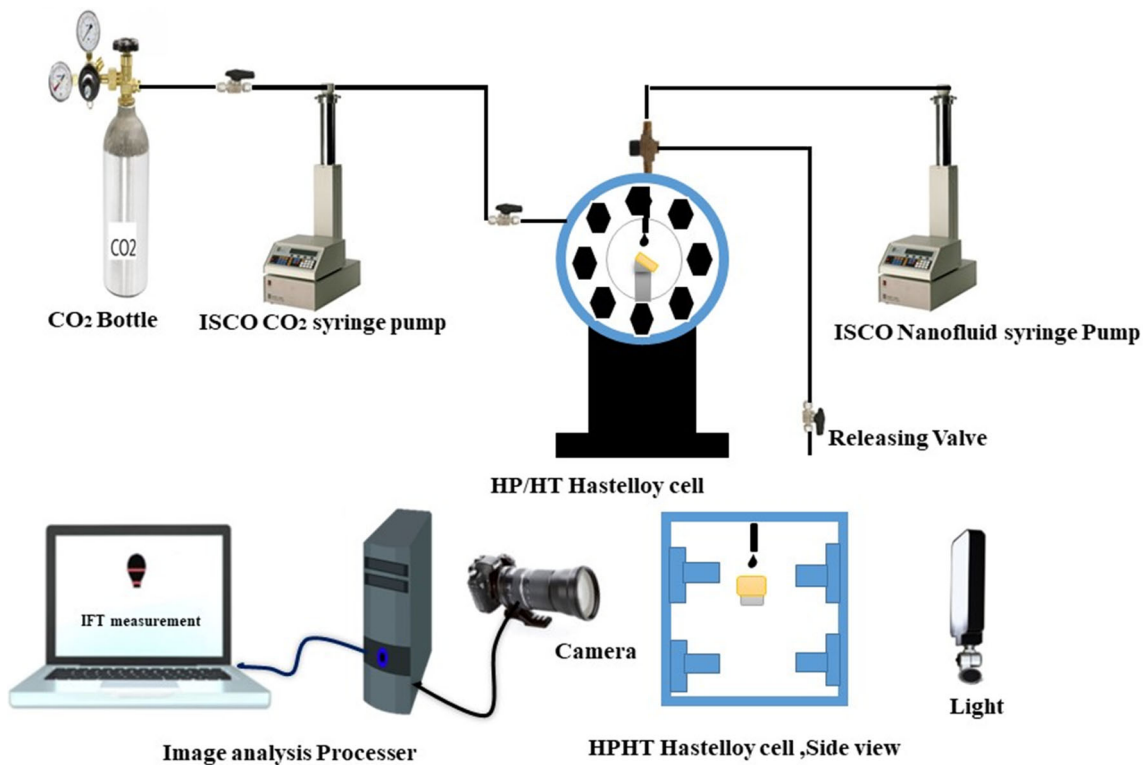
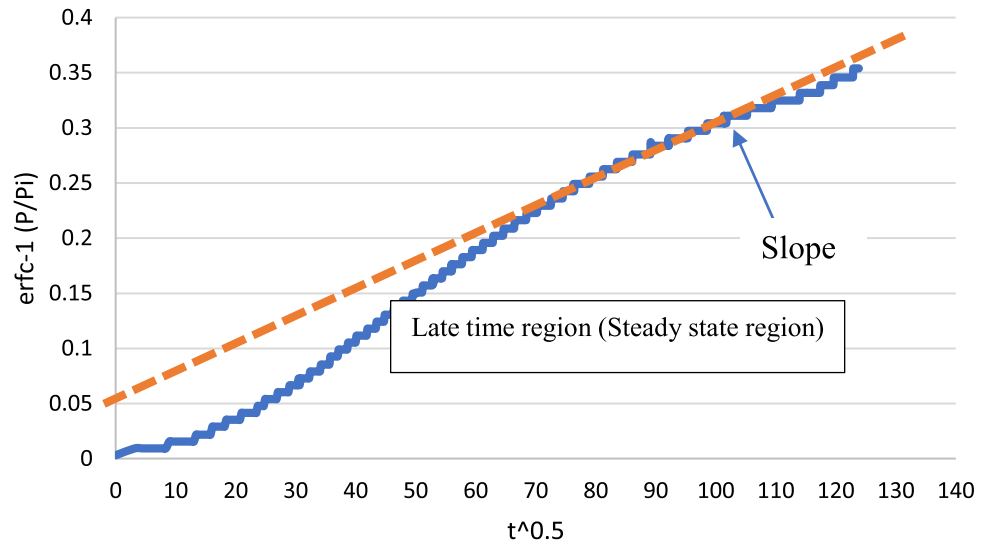


Fig. 5 Schematic diagram for measuring interfacial tension (modified after [34])

into the cell using a dispensing needle and a second, high-precision syringe pump when the pressure had settled. At the end of the dispensing needle, a drop of nanofluid was created by the second pump at a flow rate that was rather modest (0.4 ml/min), and it progressively grew in volume

until it finally dropped to the ground owing to gravity [34]. The whole procedure was monitored and recorded using a high-resolution video camera. Images from the movie files at the precise moment before the droplet went down were taken for measurements (as shown in Fig. 5).

3 Results and Dissection

3.1 Characterization of Greenly Synthesized Nanomaterials

We typically used FTIR to investigate the mineralogical composition of the NPs and nanocomposite, aiming to determine the accuracy of the NPS. Additionally, we employed Fast Emission Scanning Electron Microscope (FE-SEM) technology to characterize the various sizes and forms of NPS or NCs. Furthermore, a thermogravimetric analysis calculation, known as a TGA, was carried out to investigate the prepared NPs' thermal stability and nanocomposite at temperatures ranging from 25 to 300 °C. The interaction of SiO₂ NPs with Xanthan was studied using FTIR spectroscopy. As shown in Fig. 6, the peak at 471.52 cm⁻¹, which corresponds to the symmetric stretching vibrations of the Si–O–Si bonds, can be used to identify silica formation. Peaks at 643.98 cm⁻¹ are caused by SiO₄ tetrahedron vibration [43, 44]. The band of about 808 cm⁻¹ corresponds to Si–O bending vibration, in which oxygen moves perpendicular to the Si–Si lines in the Si–O–Si plane. The absorption at 945 cm⁻¹ is caused by Si–OH bending vibration [44]. The band at 1108.3 cm⁻¹ corresponds to an asymmetric stretching vibration of the Si–O–Si band. The bridging oxygen atom travels parallel to the Si–Si lines in the opposite direction as its Si neighbors. Stretching vibrations of the COO– group are responsible for the two peaks at 1418.05 cm⁻¹ and 1573 cm⁻¹. Another two peaks at 2911 and 3427 cm⁻¹ correspond to CH and Si–OH stretching vibrations, respectively. The disappearance of the signal at 1734 cm⁻¹ suggests that XG produced the silica particles.

The FE-SEM micrograph and particle size distribution of the SiO₂ NPs and SiO₂/Xanthan NCs produced are shown in Fig. 7a. The surface morphology of SiO₂ is regular, smooth spherical. The NPs are 30–70 nm in diameter. The tiny particles' increased concentration of OH groups causes a decrease in the rate of the condensation and hydrolysis reactions, which prevents the formation of the bigger particles. So, by changing the quantity of ethanol, it is possible to regulate the powder's particle size and particle size distribution [44]. Additionally, the FE-SEM shown in Fig. 7b illustrates the morphology of the produced NCs. In reality, internal pores are present, and Xanthan's production of silica particles caused the surface roughness to grow. According to SEM data, the homogeneous green NCs have some agglomeration and a semi-spherical shape.

X-ray diffraction (XRD) was employed to determine the mineralogical composition of SiO₂ NPs and SiO₂/Xanthan NCs, while thermogravimetric analysis (TGA) was used to study their thermal properties. Figures 8 and 9 display a customary X-ray diffraction (XRD) pattern and thermogravimetric analysis (TGA) spectrum for nano-silica.

Figure 8 displays an XRD spectrum that shows distinct peaks representing the crystalline planes of both xanthan and SiO₂ NPs. These peaks indicate the crystallinity and purity of these materials. Notably, the XRD pattern does not reveal any extra diffraction peaks from metallic impurities. This finding strongly suggests that the synthesized sample has a high level of phase purity and is devoid of noteworthy metallic impurities.

Thermogravimetric analysis (TGA) was employed to assess the thermal characteristics of nano-structured silica (SiO₂). The TGA results, presented in Fig. 9 for SiO₂ NPs and SiO₂/Xanthan nanocomposites, reveal a weight loss peak between the initial temperature and 170 °C, constituting only 20% of the total weight loss. TGA indicates that the structure of SiO₂ NPs remains unchanged throughout this temperature range. Subsequently, at 300 °C, the nano-structured silica experiences a weight shift of around 60%, diminishing to 25% at 600 °C. The most substantial weight loss observed in the TGA analysis of SiO₂ NPs and SiO₂/Xanthan nanocomposites primarily occurs in the third region (600 °C), accounting for approximately 76.36% and 73.3%, respectively.

3.2 Diffusion Coefficient

3.2.1 Validation Results

This study compared the experimental results obtained and the data reported by Jafari Raad et al. [13] for CO₂/brine (200 gm/l NaCl) at 853 psi and 40 °C. The reported diffusion coefficient by Jafari Raad et al. [13] was 2.59×10^{-9} m²/s, while the diffusion coefficient of CO₂ into brine under the same conditions was measured to be 2.15×10^{-9} m²/s. This result demonstrates good agreement with the previously reported value.

In this study, we conducted experiments to explore how NPs affect the diffusion of CO₂ in a brine solution. Our analysis of the results involved the calculation of the diffusion coefficient based on the slope of the P–T curve obtained in later stages. We investigated several parameters, including NP concentration, brine concentration, temperature, and pressure, to determine how they influence the pressure decay curves. We will discuss the impact of each of these parameters in detail below.

3.2.2 Impact of Silica NPs on CO₂ Diffusion Coefficient

As per the findings presented in Fig. 10a, we compared the pressure reduction over time for NaCl brine solutions with and without SiO₂ nanofluid. The results indicated that the diffusion coefficient of CO₂ significantly increased from 2.1497×10^{-9} m²/s (in the absence of NPs) to 4.8681×10^{-9} m²/s at a concentration of 0.1 wt.% of SiO₂ NPs. We made these

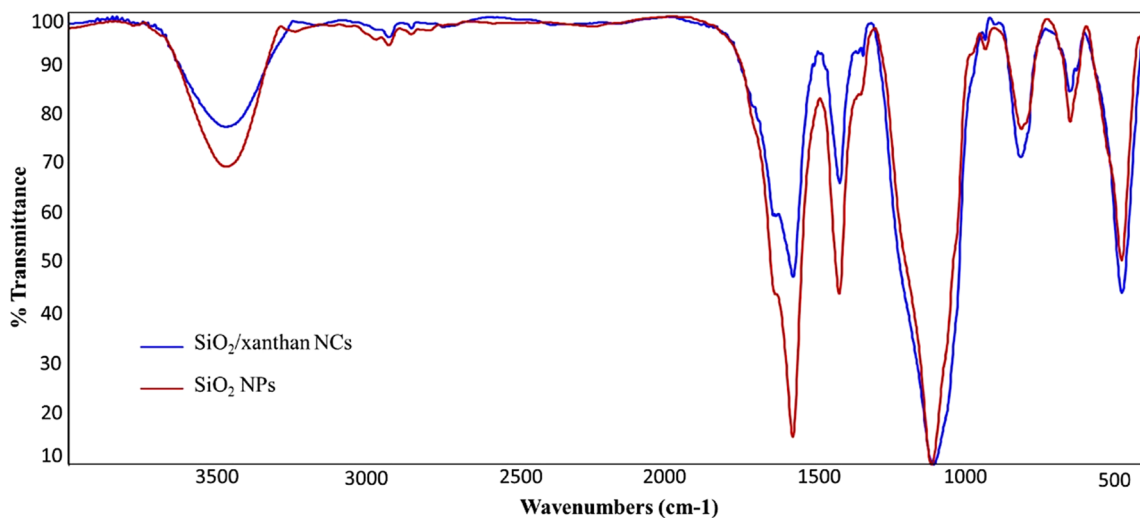


Fig. 6 FTIR of synthesized silica nanoparticle and SiO₂/Xanthan NCs

Fig. 7 Depicts FE-SEM micrographs showing the size distribution of; **a** SiO₂ NPs and **b** SiO₂/Xanthan NCs

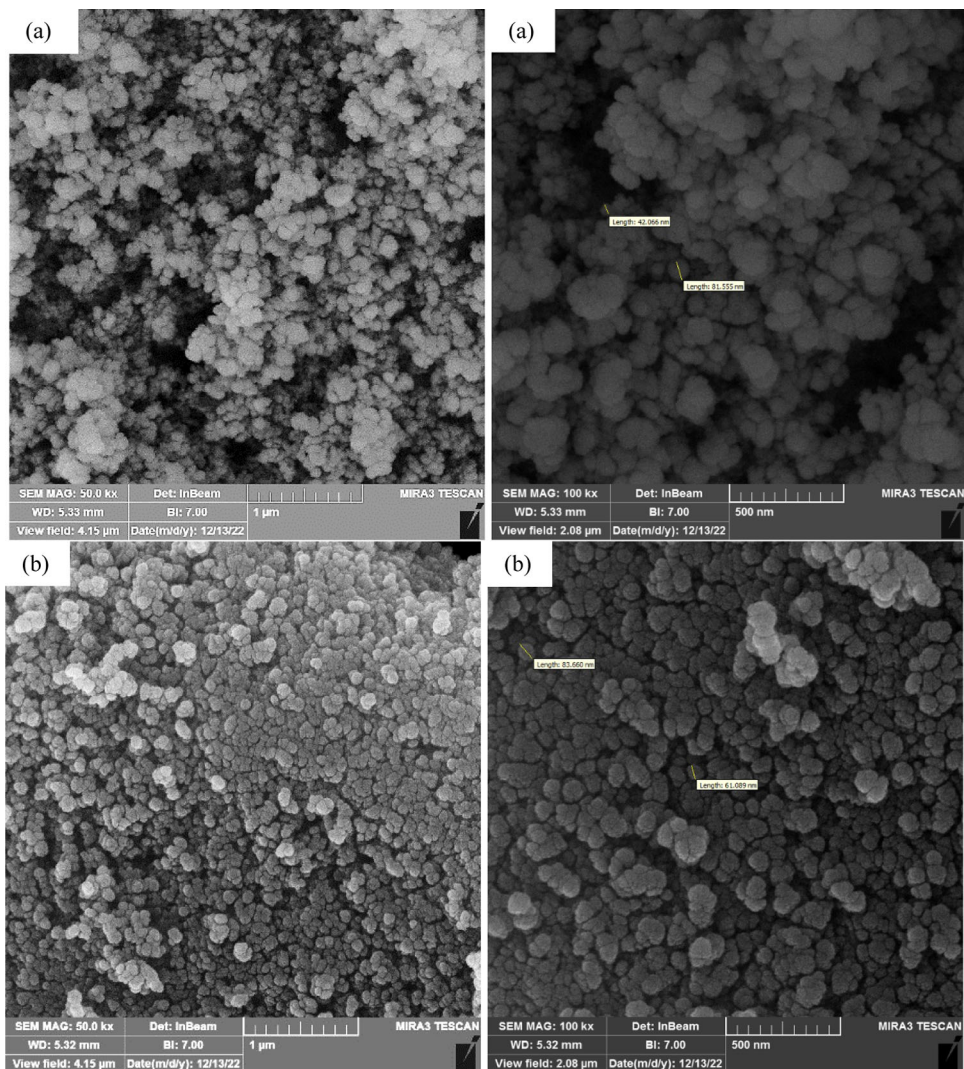


Fig. 8 XRD pattern of the synthesized SiO₂ NPs and SiO₂/Xanthan NCs

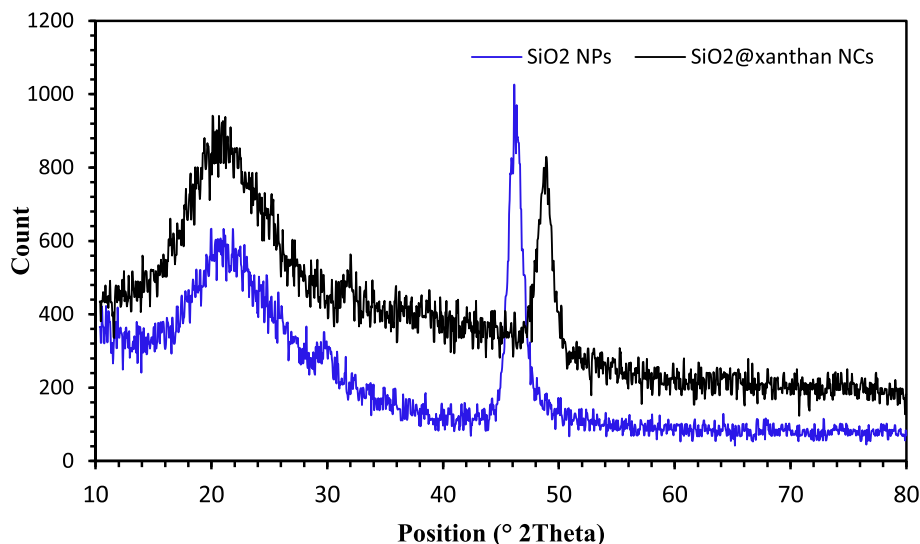
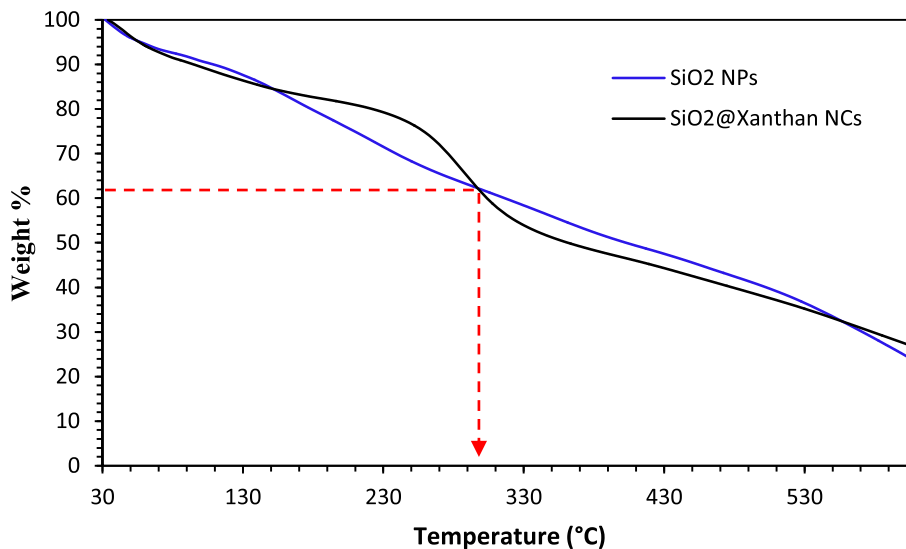


Fig. 9 Thermal gravimetric analysis (TGA) pattern of the synthesized SiO₂ NPs and SiO₂/Xanthan NCs



observations under controlled conditions of 853 psi and 40 °C (as given in Table 2).

We examined the potential impact on the diffusion of CO₂ by using 0.1 wt.% of SiO₂/nanofluids, where we suspended SiO₂ NPs in a NaCl brine base fluid. The relationship between enhancements in CO₂ diffusion and the application of nanofluids was a multifaceted and dynamic field of investigation characterized by numerous variables that impacted the overall phenomenon. The following points were taken into consideration: The optimal dispersion of NPs in a nanofluid is a critical factor in enhancing diffusion. We are attaining homogeneous dispersion and inhibiting the settling or clustering of SiO₂ particles and had been crucial to optimize the enhancements in potential diffusion. The addition of SiO₂ NPs in the nanofluid resulted in a synergistic impact with the underlying fluid, resulting in improvements in diffusion. NPs have the ability to modify the thermophysical properties of

fluids, which may include augmenting thermal conductivity or altering surface tension. The alterations have the potential to impact the diffusion of CO₂ in an indirect manner. Silicon dioxide NPs exhibit a greater surface area, affording more adsorption sites for carbon dioxide molecules. This phenomenon can potentially impact their diffusion characteristics. The potential enhancement of CO₂ diffusion may be attributed to the increased surface area in this context. The shape and porosity of NPs can influence the diffusion enhancement. SiO₂ NPs with precisely defined structures and regulated morphologies had the potential to establish conduits and interlinked apertures that expedite the process of CO₂ diffusion. Enhancing the NPs' morphology can potentially improve the diffusion coefficient of CO₂.

It is imperative to acknowledge that the association between the attributes of nanofluids and the enhancements

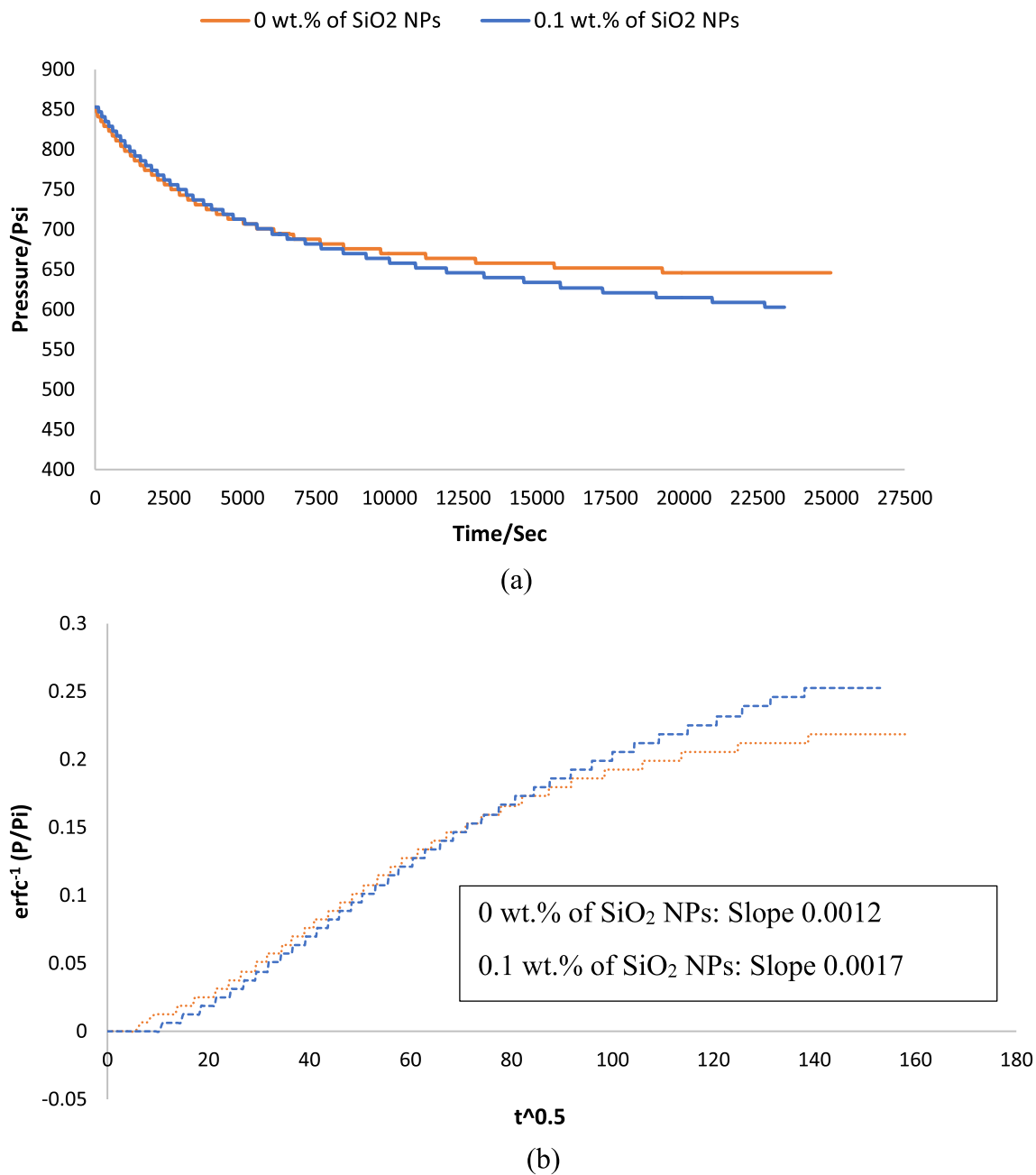


Fig. 10 Effect of SiO₂ NPs on CO₂ diffusion in 20 wt.% NaCl brine with 0.1 wt.% silica-brine nanofluid (40 °C and 853 psi); **a** Measured pressure decay data as a function of time, and **b** $\text{erfc}^{-1}(P/P_i)$ versus $t^{0.5}$

in CO₂ diffusion may be subject to the influence of additional variables, including but not limited to temperature, pressure, and the particularities of the experimental configuration. Moreover, the interplay between NPs and carbon dioxide exhibits intricate characteristics, and the underlying mechanisms dictating the improvements in diffusion may differ based on the nanoparticle composition, surface characteristics, and the type of interaction between carbon dioxide and NPs.

3.2.3 Impact of Nanomaterials on CO₂ Diffusion Coefficient Under Different Conditions of SiO₂ Concentration, Pressure, and Temperature

The experimental study described in Sect. 2.3 monitored the diffusion process of CO₂ into NaCl brine (200gm/L of deionized water) and nanofluids. Multiple tests were conducted, as listed in Table 2, with different concentrations of SiO₂ NPs (0.05, 0.1, and 0.25 wt.%) at various temperatures and pressures. The aim was to investigate the influence of

Table 2 Calculated CO₂ diffusion coefficients at different SiO₂ NPs concentrations, pressure, and temperature conditions

Exp. #	Pressure (psi)	Temperature °C	Partial pressure (Psi)	Z factor	Diff. coefficients m ² /s × 10 ⁻⁹	SiO ₂ NPs composition
1	725	30	604	0.704	5.563	0.1 wt.% SiO ₂ NPs
2	853	40	615	0.687	4.861	0.1 wt.% SiO ₂ NPs
3	950	50	723	0.693	0.944	0.1 wt.% SiO ₂ NPs
4	725	30	630	0.704	3.157	0.05 wt.% SiO ₂ NPs
5	853	40	707	0.687	4.009	0.05 wt.% SiO ₂ NPs
6	950	50	766	0.693	4.241	0.05 wt.% SiO ₂ NPs
7	725	30	655	0.704	2.318	0.25 wt.% SiO ₂ NPs
8	853	40	738	0.687	2.796	0.25 wt.% SiO ₂ NPs
9	950	50	858	0.694	0.519	0.25 wt.% SiO ₂ NPs
10	725	40	603	0.747	0.971	0.1 wt.% SiO ₂ NPs
11	853	30	757	0.622	2.022	0.1 wt.% SiO ₂ NPs
12	853	50	656	0.733	2.643	0.1 wt.% SiO ₂ NPs
13	950	40	664	0.634	2.516	0.1 wt.% SiO ₂ NPs
14	853	40	627	0.687	2.149	0 wt.% SiO ₂ NPs

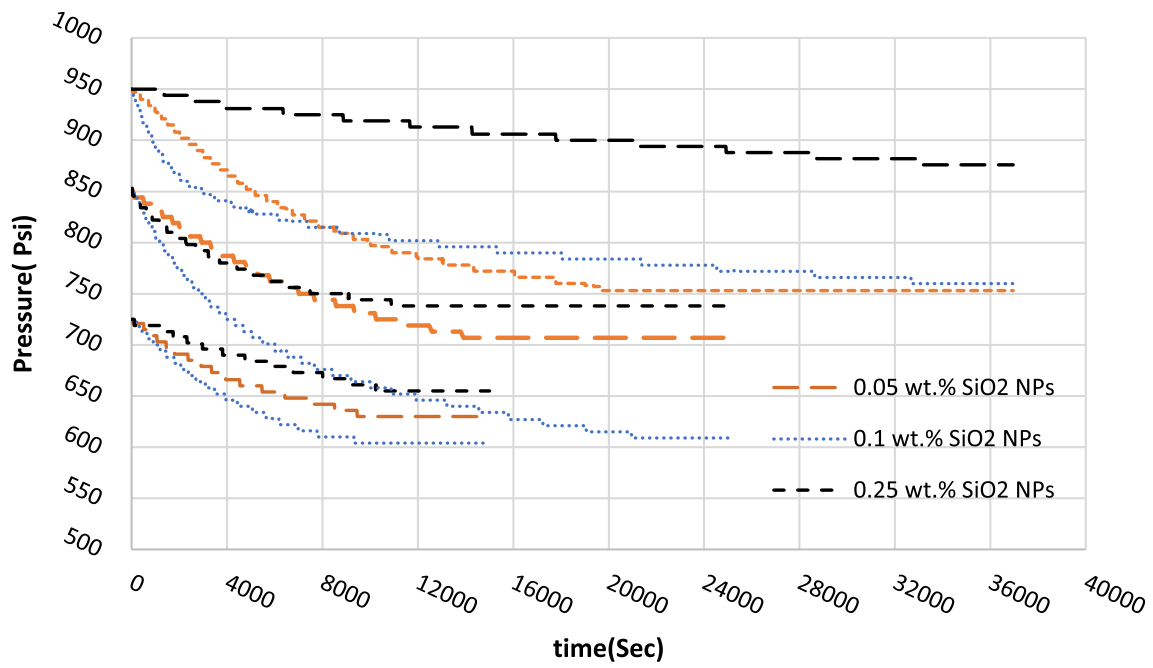
nanofluid concentration on the diffusion coefficient. Pressure decay measurements were obtained by analyzing the shifting curves of pressure fluctuation with time and the $t^{0.5}$ with $\text{erfc-1}(P/P_i)$ curve for each concentration. Figures 11 and 12 illustrate the impact of varying SiO₂ nanoparticle concentrations on the diffusion coefficients of CO₂ under different pressure and temperature conditions. Figure 11a, b shows a decrease in the gradient of the curves, indicating that the concentration of CO₂ gas in the liquid phase starts weak and increases throughout the experiment. Consequently, there is a relatively higher initial pressure drop during the early stages of the investigation due to the rapid diffusion of gas into the liquid.

Figure 12 provides compelling evidence of the significant influence of nano-silica concentration on the diffusion coefficient of CO₂. The results indicate that increasing the concentration from 0.05 to 0.1 wt.% yields an optimal concentration at 30 °C and 40 °C and pressures of 725 and 853 psi, respectively. However, when the nanofluid concentration exceeds 0.1 wt.%, the CO₂ diffusion decreases due to

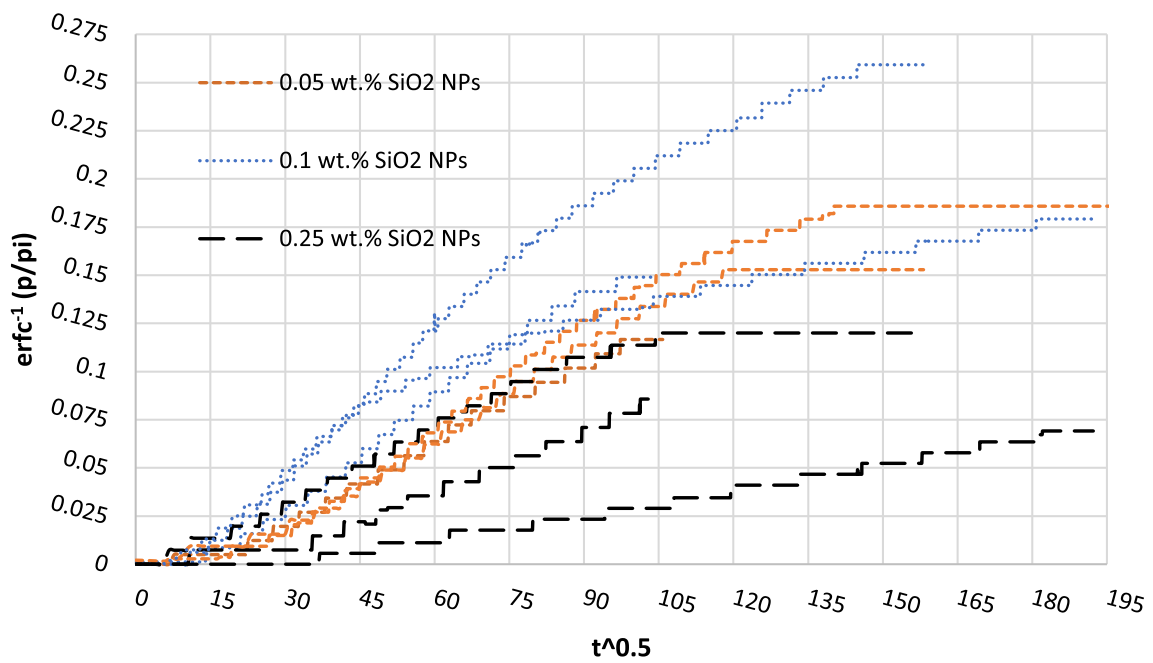
an increase in nanofluid viscosity and a decrease in Brownian motion. This change is reflected in a steeper slope of the curves, indicating a more pronounced impact on the diffusion coefficient of CO₂ in the nanofluid.

NPs primarily enhance mass transfer through the grazing effect and Brownian motion. According to the grazing effect theory [45], the presence of NPs at the gas–liquid interface leads to the adsorption and subsequent desorption of gas molecules in the liquid phase, thereby increasing the mass transfer rate. As the concentration of nanofluids increases, more NPs are available at the fluid boundary layer, enhancing the grazing effect. On the other hand, the Brownian motion hypothesis suggests that NPs' random motion induces micro-convections in the liquid, creating a disturbance field that can enhance the effective mass diffusion of absorbed components.

Figure 12 illustrates that the addition of 0.1 wt.% SiO₂ NPs saturates the surface of the bubbles with additional particles, diminishing the grazing phenomenon. Moreover, an increase in nanofluid viscosity results in the dissipation of



(a)



(b)

Fig. 11 The impact of varying SiO₂ NPs concentration on CO₂ diffusion under different pressure and temperature conditions: **a** measured pressure decay data as a function of time and **b** $t^{0.5}$ versus $erfc^{-1}(p/pi)$

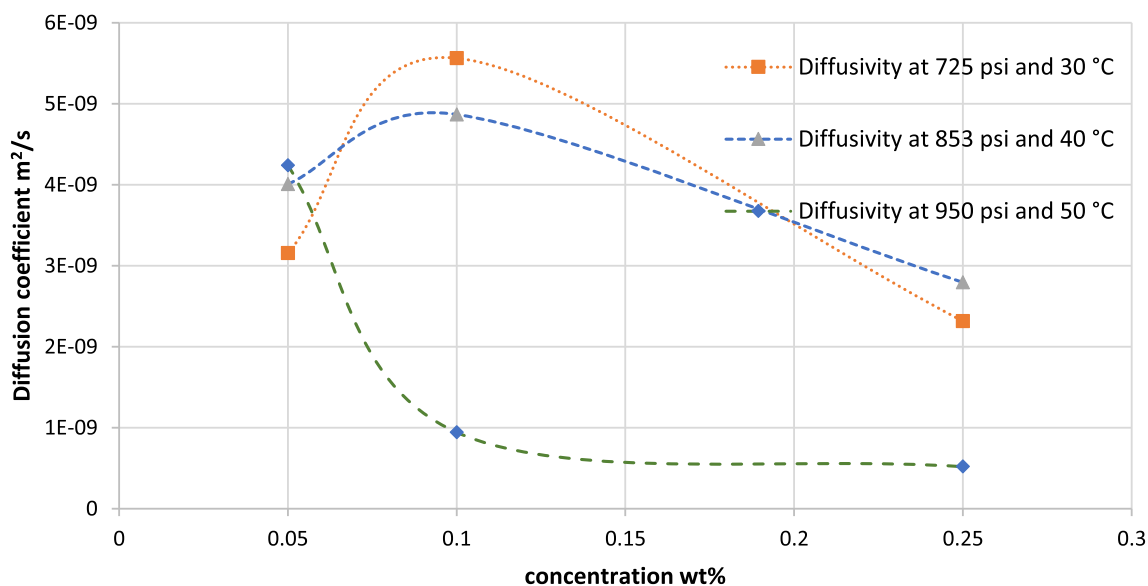


Fig. 12 CO₂ diffusion coefficient at different conditions and SiO₂ NPs concentrations

nanoparticle-driven micro-convections, reducing Brownian motion and CO₂ diffusion. Recent studies have shown that incorporating NPs into the base fluid can affect diffusion, which depends on various factors such as viscosity, surface tension, intermolecular forces, and physical characteristics of the particles. An increase in fluid viscosity hampers micro-convection, consequently reducing the diffusion of CO₂ in nanofluids.

To examine the impact of nanofluid pressure on the diffusion of CO₂, we conducted a study under specific experimental conditions. These conditions included a temperature of 40 °C, a concentration of 0.1 weight percent of SiO₂ NPs, and pressure levels of 725 psi, 853 psi, and 950 psi. We performed the tests using a nanofluid composed of a base fluid of 200g/l NaCl brine. Figures 13 and 14 depicts the pressure versus time curve, $t^{0.5}$ with $\text{erfc}^{-1}(p_i/p)$, and the diffusion coefficients obtained from the experiments.

Figure 13 shows the pressure decay curves for the CO₂/nanofluid system at various initial pressures. When the initial pressure is raised from 725 to 853 psi, there is a noticeable increase in the initial slope of the curves for nanofluids containing 0.1 wt.% SiO₂ NPs. However, at 950 psi, the slope starts to decrease. This indicates that as the pressure rises, we can expect a gradual increase in the diffusion coefficient of CO₂. Figure 14 demonstrates that the diffusion coefficient of CO₂ in the nanofluid consistently rises as the pressure increases. Elevated pressure serves as a driving force for gas molecules, facilitating faster diffusion and counteracting the viscosity increase in CO₂, which would otherwise impede diffusion. Consequently, the impact of pressure on the diffusion coefficient is relatively small. Furthermore, higher

pressure leads to reduced equilibrium attainment time or diffusion duration. However, as pressure increases further, the viscosity of the gas increases, resulting in a decrease in the diffusion coefficient of CO₂. Therefore, once a specific pressure threshold is reached, the influence of pressure on the diffusion coefficient diminishes.

It is important to note that the specific effect of nanofluid pressure on CO₂ diffusion coefficient is highly dependent on various factors, such as the properties of the nanofluid, the characteristics of the NPs, and the experimental conditions. Additionally, the relationship between pressure and CO₂ diffusion coefficient may not be linear, and it can vary based on the specific nanofluid composition and system characteristics.

Three separate experiments were conducted at 30, 40, and 50 °C to investigate the impact of temperature. The experimental conditions included a pressure of 853 psi and a concentration of 0.1 wt.% of SiO₂ NPs. The results of these experiments, depicting the decrease in CO₂ pressure over time as a function of temperature, are shown in Figs. 15 and 16.

Figure 15 demonstrates the pressure decay of CO₂ for the 0.1 wt.% silica nanofluid at 853 psi at different temperatures. The slope of the curve increases as the liquid temperature rises from 30 to 40 °C. As shown in Fig. 16, an increase in temperature enhances the diffusion of CO₂ in nanofluids. This can be attributed to higher temperatures resulting in increased kinetic energy of gas molecules, leading to a faster rate of gas entry into the nanofluid. Conversely, as temperature increases, the viscosity of the liquid decreases, affecting the rate at which gas molecules can enter the liquid phase.

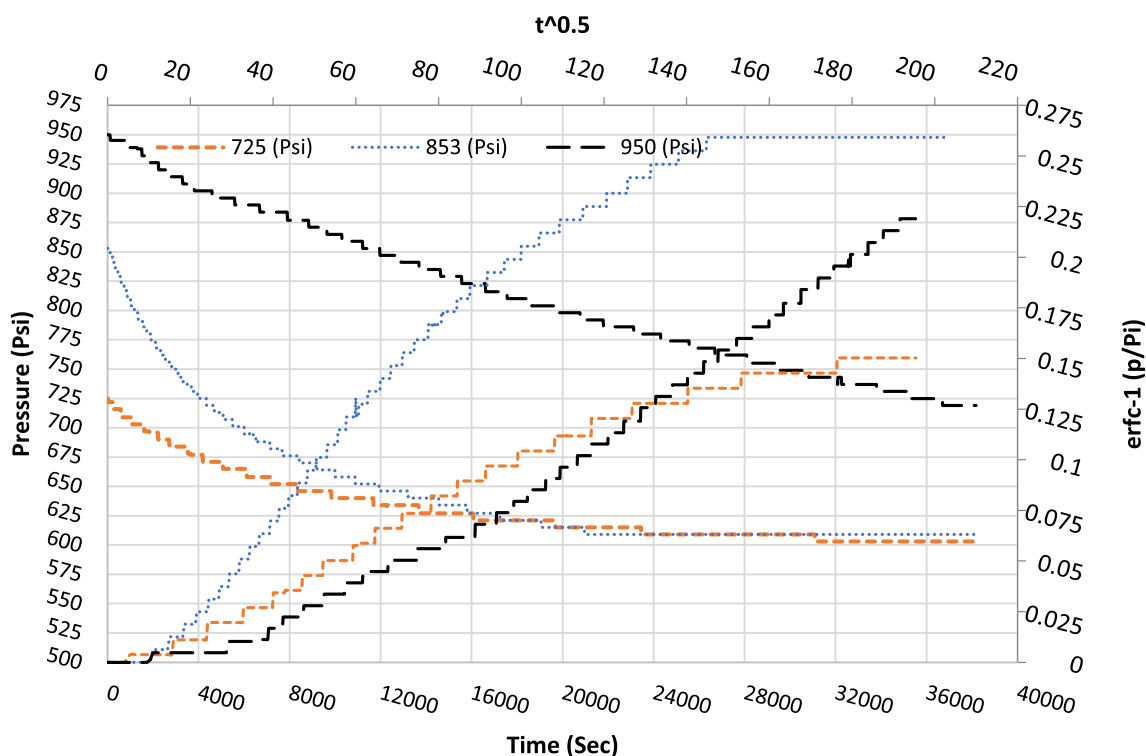
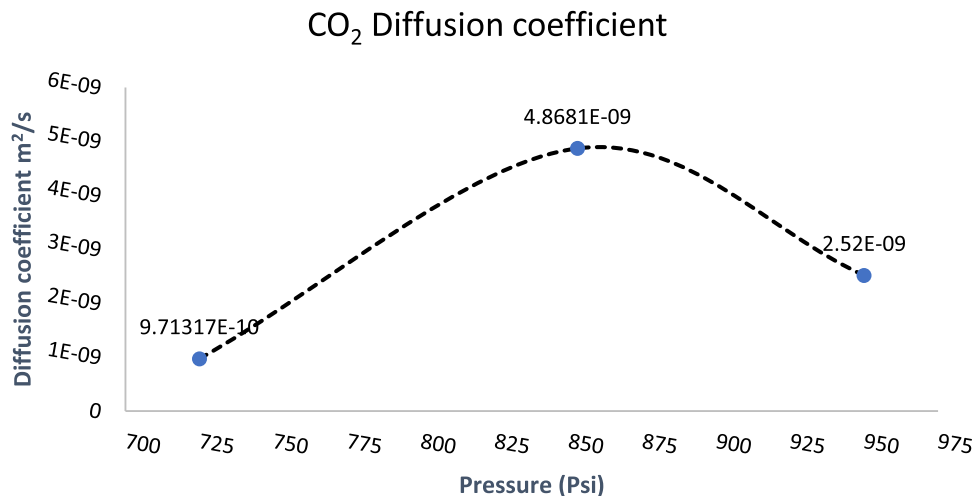


Fig. 13 Pressure decay curve of CO₂/nanofluid at different pressures under the same concentration and temperature

Fig. 14 Effect of pressure on CO₂ diffusion coefficient (at 0.1 wt.% of SiO₂ NPs and 40 °C)



Therefore, increased kinetic energy and decreased viscosity can explain water’s increased CO₂ diffusion coefficient with rising temperature.

Moreover, when the liquid temperature increases from 40 to 50 °C, it can increase the viscosity of CO₂ gas. Higher temperatures can cause gas molecules to move more rapidly, increasing their collisions with other gas molecules and potentially leading to a denser arrangement and higher viscosity. Additionally, elevated temperatures can inhibit the diffusion process by reducing the solubility of CO₂ in the nanofluid. As the temperature rises, the solubility of gases

generally decreases, including CO₂. This reduction in solubility can limit the availability of CO₂ molecules in the fluid, thereby hindering their diffusion.

It is important to note that various factors, such as the composition and properties of the nanofluid and the specific interactions between CO₂ and the fluid, can influence the effects of temperature on viscosity and solubility. Therefore, the exact behaviors may vary depending on the specific system and conditions.

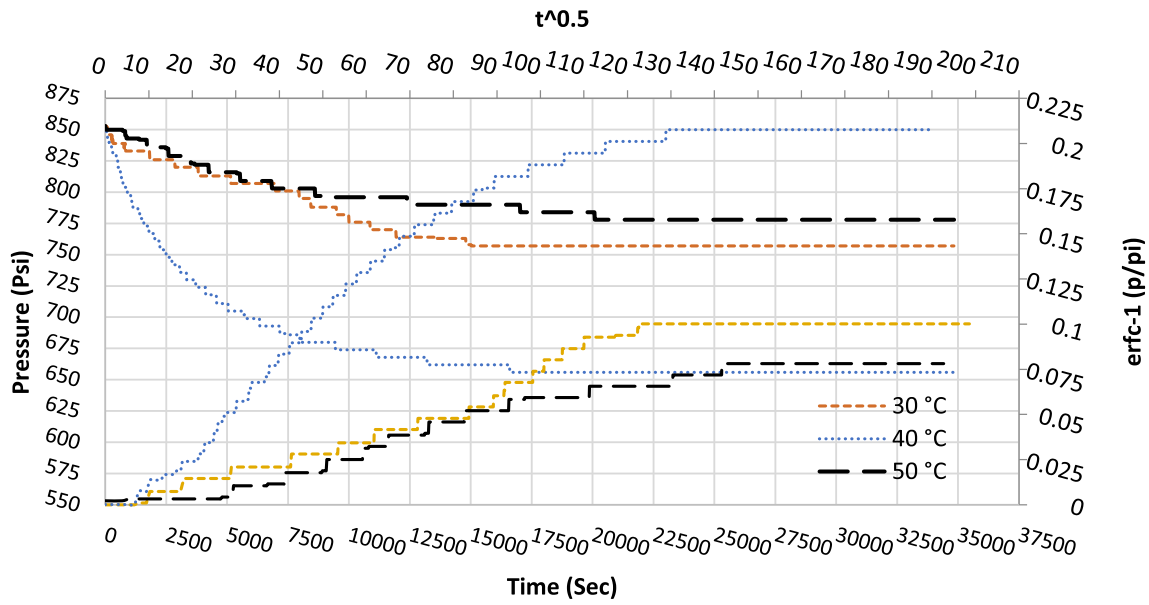


Fig. 15 Pressure decay curve of CO₂/nanofluid at different temperatures when the concentration and pressure are constant

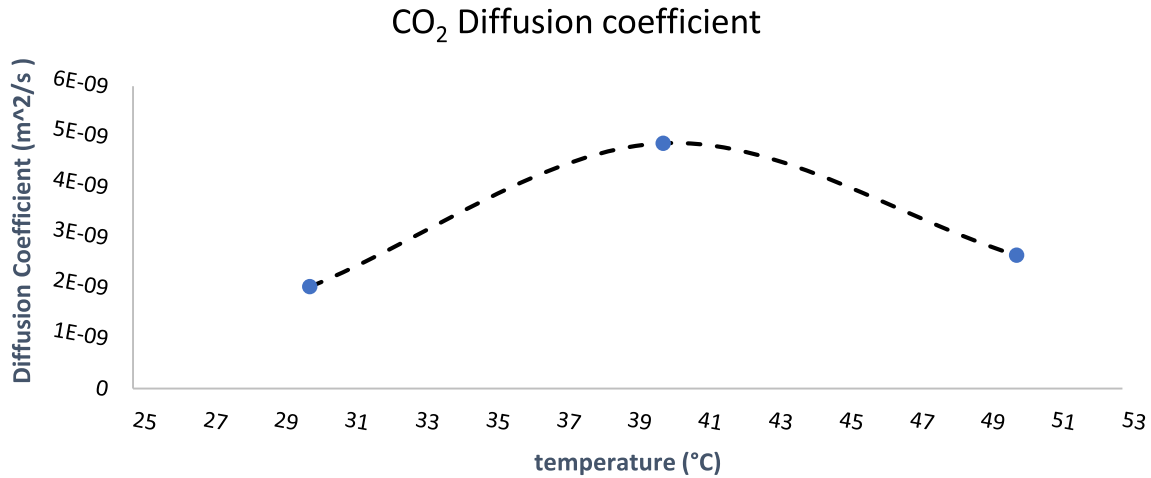


Fig. 16 Effect of temperature on CO₂ diffusion (at 0.1 wt.% of SiO₂ NPs and 853 Psi)

3.2.4 Effect of Brine Salinity on CO₂ Diffusion Coefficient

This study conducted three experiments using different NaCl salt concentrations (5 wt.%, 10 wt.%, and 20 wt.%) in a 0.1 wt.% SiO₂ nanofluid to examine their impact on the diffusion coefficient. We conducted the experiments at a pressure of 853 psi and a temperature of 40 °C. Through the analysis of the collected data, we determined a series of diffusion coefficients. In Fig. 17a, the observed trend indicates a more significant decline in pressure in the early time. The higher salinity reduces the solubility of CO₂ compared to lower concentrations. The steeper slope of the pressure decay curves in the 5 wt.% NaCl brine experiment indicates a faster pressure drop than the 20 wt.% NaCl brine experiment. This steeper

slope signifies that the CO₂ diffusion is higher in low salinity conditions than in briny formation.

According to Fig. 17b and Table 3, it is evident that an increase in total dissolved solids (TDS) leads to a decrease in the diffusion coefficient of CO₂. This decrease can be attributed to the fact that higher salinity reduces the solubility of CO₂ and increases the viscosity of the saltwater, both of which impede CO₂ diffusion. Consequently, selecting a layer with lower salinity is preferable when choosing the brine placement. The presence of dissolved salts in the brine can interact with CO₂ molecules, hindering their movement through the medium. This interaction can result in the formation of ion pairs between CO₂ and the salts, reducing the mobility of CO₂ molecules and lowering the diffusion coefficient.

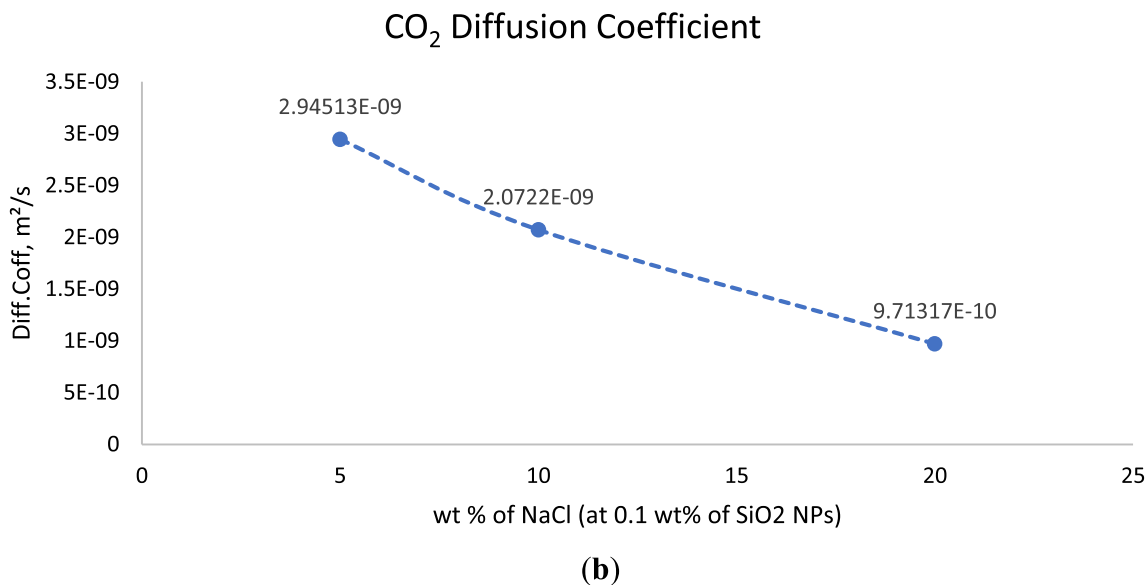
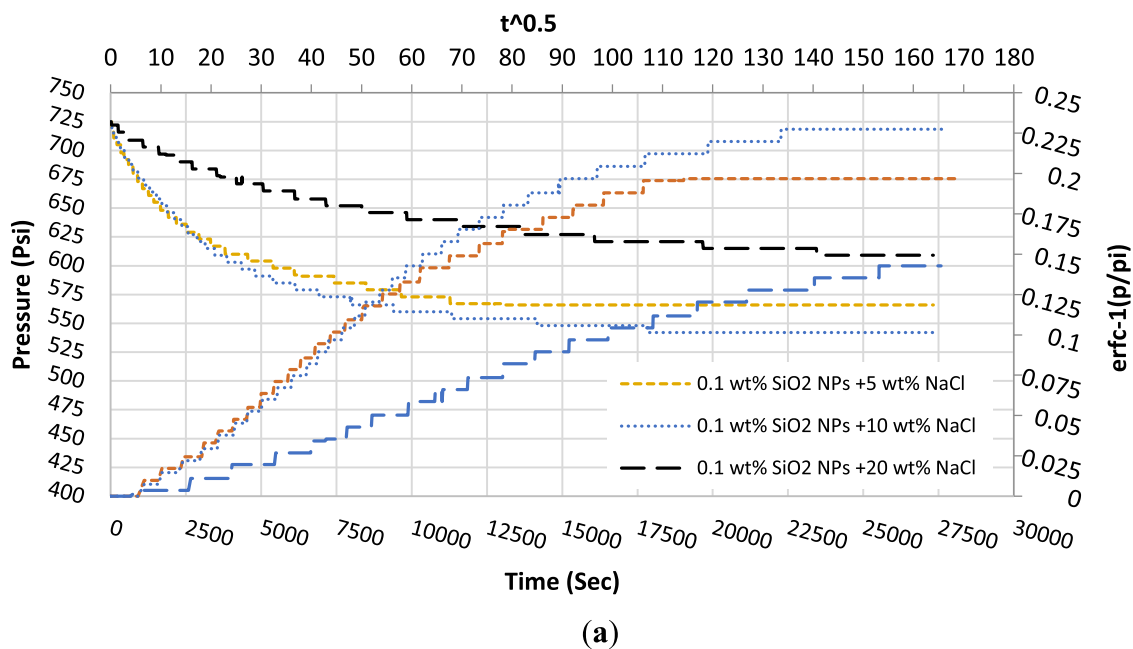


Fig. 17 a, b Effect of brine salinity on CO₂ diffusion coefficient

Table 3 Calculated CO₂ diffusion at different NaCl salt concentrations

Exp #	Pressure (psi)	Temperature °C	Partial pressure (Psi)	Z factor	Diff. coefficients × 10 ⁻⁹	Note
1	725	40	603	0.748	0.971	0.1 wt.% SiO ₂ NPs + 20 wt.% of NaCl
2	725	40	542	0.748	2.072	0.1 wt.% SiO ₂ NPs + 10 wt.% of NaCl
3	725	40	560	0.748	2.945	0.1 wt.% SiO ₂ NPs + 5 wt.% of NaCl

3.2.5 Effect of Pressure and Temperature on CO₂ Diffusion Coefficient at Supercritical Conditions

The experimental results for pressure decay runs are depicted in Fig. 18a, b. These tests were carried out at constant temperatures and nanofluid concentrations of 35 °C and 0.1 wt.% SiO₂ NPs/10 wt.% NaCl salt, with 1100 psi and 1134 psi pressures. As the pressure increases from 1100 to 1134 psi, the slope of the curve becomes steeper. This observation suggests that the diffusion coefficient (D) increases with rising pressure. This curve can be explained by increasing pressure pushing the gas molecules, compelling them to enter the nanofluid faster.

Figure 18a displays the CO₂ pressure decline over time and temperature variations for a 0.1 wt.% SiO₂ nanofluid. An increase in liquid temperature from 32 to 35 °C leads to a steeper slope in the pressure decline curve. However, the changes in the diffusion coefficient with increasing temperature and pressure are relatively smaller, as observed in Fig. 18b. This indicates that the effect of temperature becomes less significant at higher pressures, particularly around the critical pressure of CO₂. Consequently, the system becomes less sensitive to temperature, and high temperatures render the system more independent of pressure.

3.2.6 Impact of SiO₂/Xanthan Nanocomposite on CO₂ Diffusion Coefficient

Xanthan gum, a high molecular weight polysaccharide, is commonly employed as a thickening and stabilizing agent in various applications such as food, medication, and oil drilling. However, it does not directly influence the diffusion coefficient of CO₂. The diffusion coefficient of CO₂ refers to the rate at which CO₂ can diffuse through different mediums like air, water, or other fluids. While xanthan gum, as a thickening and stabilizer, can alter the characteristics of a fluid, its impact on the diffusion coefficient is not specific to CO₂ alone. In this section, we will explore the effects of xanthan gum in combination with a 2:1 mixture of SiO₂ NPs and aqueous xanthan nanocomposite on the diffusion of CO₂.

This research conducted several experiments to measure pressure–time data at specific temperatures, nanocomposite concentrations, and CO₂/nanofluid system pressures. The pressure decay method and Eq. (6) were utilized to investigate the diffusion coefficient. The study considered various factors that could affect the diffusion coefficient, including temperature, injection pressure, and nanocomposite concentration. In this section, eight diffusion experiments were performed and analyzed using the procedure described in Sect. 2.4. Table 4 provides each experiment's initial and final pressures and CO₂ diffusion values. The pressure decay resulting from CO₂ diffusion in the bulk nanofluid is illustrated over time in Figs. 19 and 20 with the normalized

pressure (pressure-to-initial pressure ratio) presented to facilitate comparison.

Figure 18a and b illustrates the impact of temperature (30 °C and 40 °C) and nanocomposite (NCs) concentration (0.05 wt.% and 0.1 wt.% of SiO₂/Xanthan NCs) on the CO₂ diffusion coefficient. Figure 19a shows that at a given temperature and pressure, the slope of the curve decreases as the concentration of NCs increases. This can be attributed to adding xanthan gum, which increases the nanofluid viscosity. The higher viscosity makes it more challenging for CO₂ to diffuse through the nanofluid, reducing the diffusion coefficient. A significant proportion of xanthan molecules in the NCs obstruct the diffusional pathway of CO₂ as shown in Fig. 19b.

Furthermore, a temperature-dependent change in the diffusion coefficient is observed. For 0.05 wt.% NCs concentration at 853 psi, the CO₂ diffusion coefficient decreases when the temperature rises from 30 to 40 °C; conversely, for 0.1 wt.% NCs concentration, the curve indicates an increase in the CO₂ diffusion value with a rise in temperature from 30 to 40 °C. The inclusion of SiO₂ NPs enhances the grazing action of the nanocomposite by adsorbing CO₂ onto the NPs, thereby increasing the microinjection of molecules. The findings suggest that temperature and nanocomposite concentration significantly influence the CO₂ diffusion coefficient. The addition of xanthan gum and the presence of SiO₂ NPs in the nanocomposite contribute to changes in the diffusion behavior of CO₂.

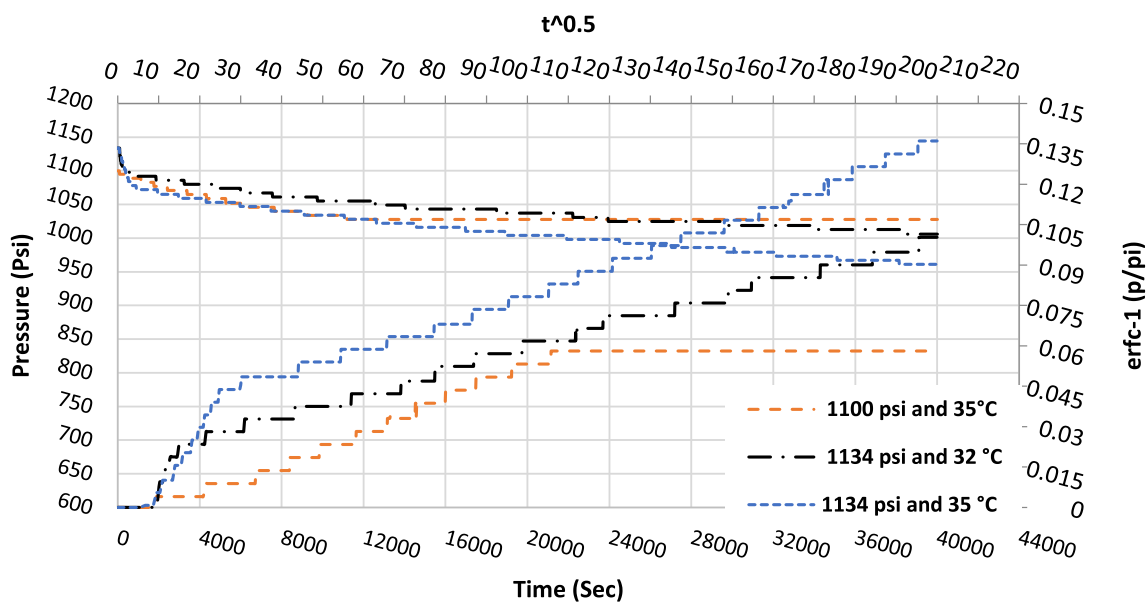
Figure 20 shows the impact of pressure on the CO₂ diffusion into nanofluid solutions with 0.05 and 0.1 wt.% of NCs, respectively. The slope of the curve rises with pressure, from 725 to 853 psi, for all combinations of temperature and concentration, as illustrated in Fig. 20. Increasing the slope also results in increased CO₂ diffusion.

3.3 IFT Measurements

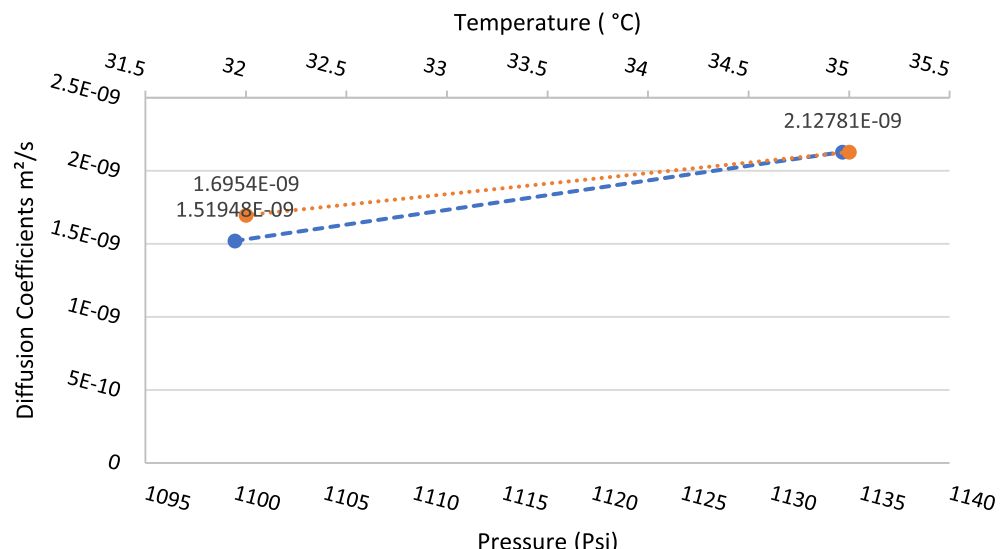
Several studies have documented the interfacial tension of CO₂–water systems [46–48]. However, there needs to be more information available on CO₂/nanofluid systems [34, 49]. The present study aimed to measure the γ values of the CO₂/nanofluid system, specifically for SiO₂ NPs and SiO₂/Xanthan nanocomposites, as a function of various parameters such as NP concentration, pressure, temperature, and salinity. The objective was to establish a comprehensive database and gain insights into the interaction properties of CO₂/nanofluid systems. The subsequent sections of this paper will delve into a discussion of the results and their potential impact on projects related to CO₂ sequestration.

3.3.1 Effect of SiO₂ NPs Concentration on CO₂/Nanofluid IFT

Adding SiO₂ NPs into a CO₂ nanofluid can potentially impact the interfacial tension (IFT) between the CO₂ and



(a)



(b)

Fig. 18 a, b Effect of pressure and temperature changes on the CO₂ diffusion at supercritical CO₂

Table 4 CO₂ diffusion coefficient for SiO₂/Xanthan nanocomposite

Exp#	Pressure (psi)	Temperature °C	Partial pressure (Psi)	Z factor	Diff. coefficients m ² /s × 10 ⁻⁹
1	725	30	636	0.704	1.904
2	725	40	634	0.748	1.074
3	853	30	617	0.622	3.731
4	853	40	737	0.688	2.343
5	725	30	691	0.704	0.359
6	725	40	639	0.748	0.273
7	853	30	770	0.622	0.413
8	853	40	755	0.688	1.301

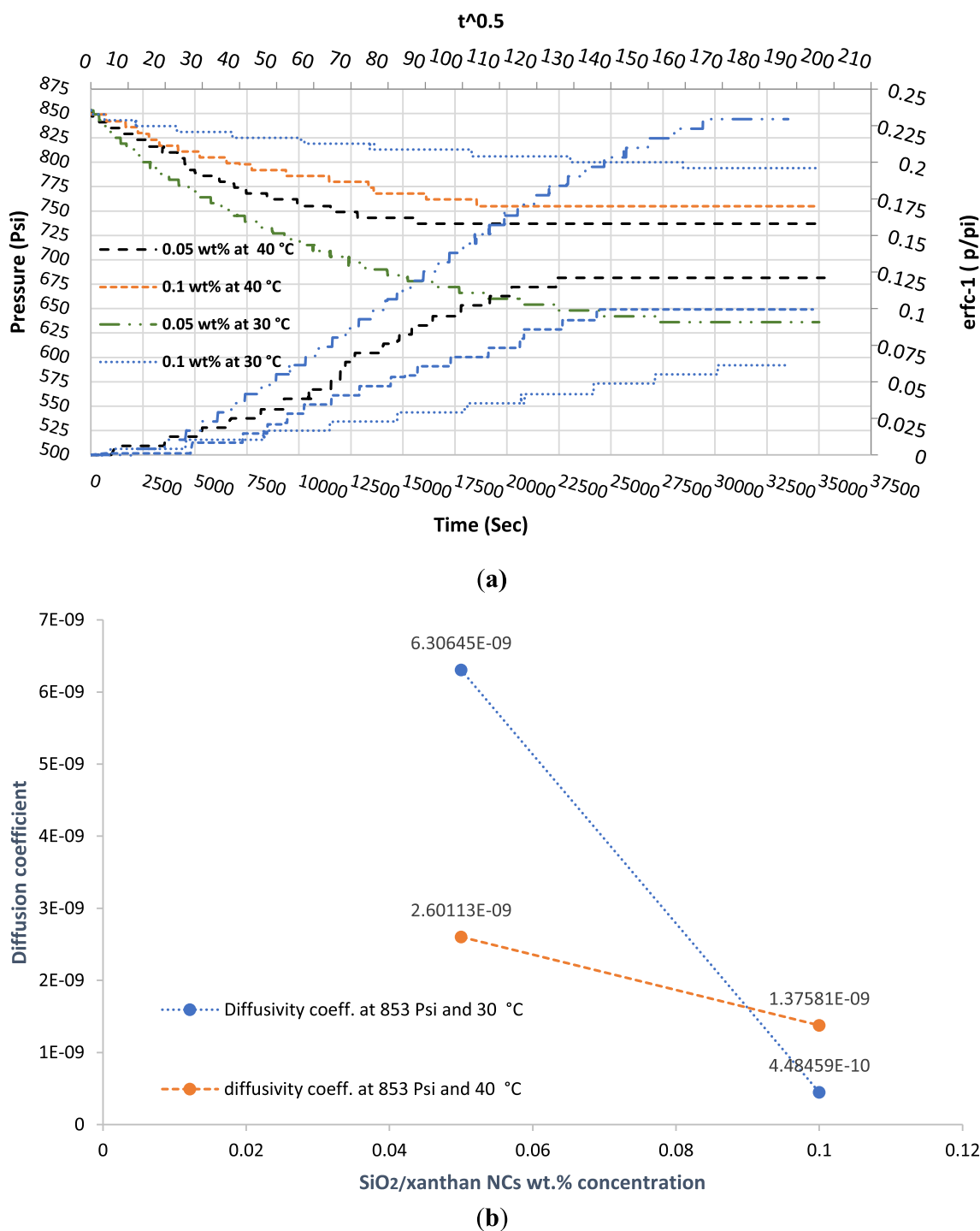


Fig. 19 a and b Effect of temperature and SiO₂/Xanthan NCs concentration on the CO₂ diffusion

the nanofluid. The interfacial tension (IFT) is commonly evaluated concerning the nanoparticle concentration, and the findings indicate a notable decline in γ as the NP concentrations increase, as illustrated in Fig. 21 and Table 5.

An increase in the NP load from 0.05 to 0.1 wt.% resulted in a reduction of γ from 1.05 mN/m to 0.855 at 725 Psi (at

30 °C) and from 1.038 to 0.912 mN/m at 853 Psi (at 40 °C). We also observed that raising the NP concentration from 0.1 to 0.25 wt.% decreased interfacial tension (IFT) from 0.943 to 0.879 mN/m at a pressure of 950 Psi and a temperature of 50 °C. However, we did not observe any further reduction in γ when increasing the NP concentration for SiO₂ NPs at

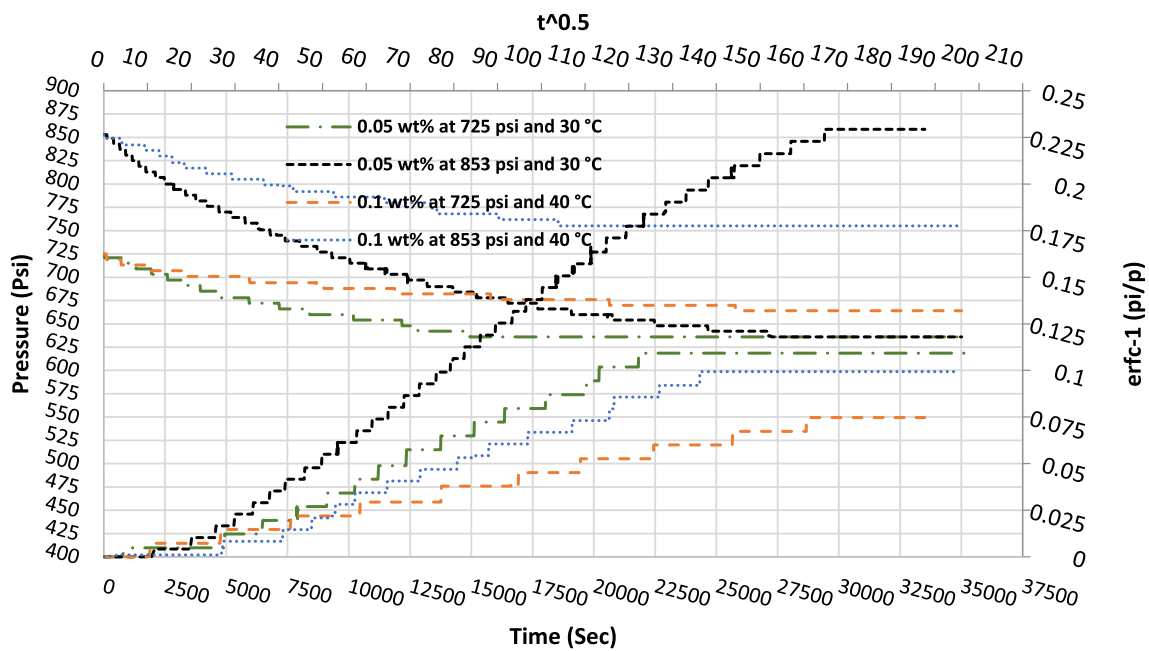


Fig. 20 Effect of pressure, temperature, and NC concentration on the CO₂ diffusion

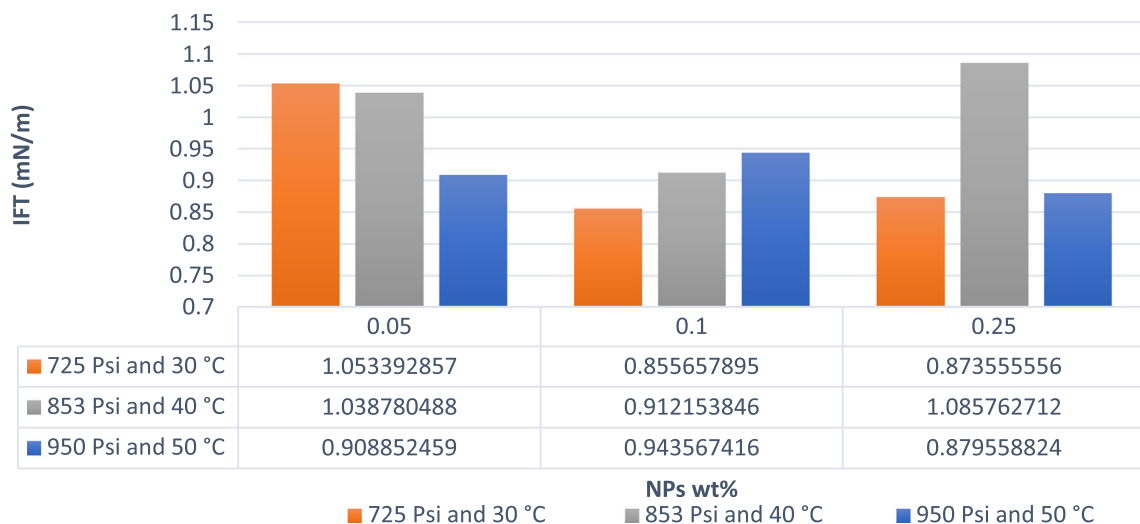


Fig. 21 Impact of SiO₂ NPs concentration on CO₂/nanofluid IFT

725 Psi and 853 Psi (at 30 °C and 40 °C), respectively, when the concentration was ≥ 0.05 wt.%. Our observations show that including SiO₂ NPs can decrease the interfacial tension (IFT) between CO₂ and the nanofluid. This phenomenon can be attributed to the shuttle effect mechanism, where the NPs accumulate at the interface, reducing the interfacial area.

The concentration of NPs of SiO₂ commonly influences the extent of reduction in IFT. Typically, elevated concentrations of NPs result in a more significant reduction in interfacial tension (IFT). Nevertheless, when present in exceedingly high concentrations, the NPs may initiate

aggregation and generate larger structures, potentially augmenting the interfacial tension.

3.3.2 Effect of Pressure and Temperature on CO₂/Nanofluid IFT Measurements

The effect of pressure and temperature on CO₂/nanofluid interfacial tension (IFT) measurements can depend on several factors, including the composition and properties of the nanofluid and the pressure and temperature range being considered. Consequently, this research measured CO₂/nanofluid IFT at pressure ranges 725, 853, and 950 psi

Table 5 Calculated IFT of carbon dioxide-(SiO₂) nanofluid by pendant drop methods

Exp#	Nanomaterials type	Concentration (wt.%)	Pressure Psi	Temperature °C	Average IFT value mN/m
1	Brine-CO ₂	0	853	40	44.3517
2	SiO ₂ -CO ₂	0.1	950	40	0.9016
3	SiO ₂ -CO ₂	0.25	725	30	0.8735
5	SiO ₂ -CO ₂	0.05	853	40	1.0388
6	SiO ₂ -CO ₂	0.25	853	40	1.0858
7	SiO ₂ -CO ₂	0.05	725	30	1.0534
8	SiO ₂ -CO ₂	0.25	950	50	0.8795
9	SiO ₂ -CO ₂	0.1	725	30	0.8556
10	SiO ₂ -CO ₂	0.1	853	40	0.9098
11	SiO ₂ -CO ₂	0.1	853	50	0.8096
12	SiO ₂ -CO ₂	0.1	853	30	0.9122
13	SiO ₂ -CO ₂	0.05	950	50	0.9088
14	SiO ₂ -CO ₂	0.1	950	50	0.9436
15	SiO ₂ -CO ₂	0.1	725	40	1.1247

and temperatures 30, 40, and 50 °C at constant concentration 0.1wt % of SiO₂ NPs.

At constant temperature (40 °C), we found that with increasing pressure from 725 to 950 psi, IFT decreased from 1.124 to 0.901 mN/m for CO₂/ nanofluid solutions, as shown in Fig. 22.

This observation is consistent with the literature data. Previous studies have emphasized that pressure increased the anisotropic time-averaged van der Waals attraction for water molecules toward the carbon dioxide interface [24]. Thus, the interfacial tension values were lower at high pressure.

In general, the interfacial tension between CO₂ and a nanofluid will decrease as the pressure is increased. This is due to the fact that at higher pressures, the CO₂ and nanofluid phases become more compressed, which can lead to a reduction in the interfacial area and a corresponding decrease in interfacial tension.

However, the degree of IFT reduction with increasing pressure can depend on the specific properties of the nanofluid. For example, some studies have found that increasing the pressure can have a greater effect on IFT in nanofluids with smaller particle sizes or higher nanoparticle concentrations. In addition, the temperature can also affect the pressure sensitivity of IFT measurements, with some nanofluids exhibiting greater pressure sensitivity at higher temperatures.

The IFT demonstrated a significant decrease with increasing temperature from 30 to 50 °C at constant pressure 853 Psi as demonstrated in Fig. 23. In terms of temperature, the effect on IFT measurements in CO₂/nanofluid systems can vary. Increasing the temperature decreases the IFT, especially if the nanofluid exhibits temperature-dependent surface properties. This reduction in IFT as temperature increases from

30 to 50 °C attributed to the increased thermal energy, which facilitates the mobility and rearrangement of molecules at the interface, leading to a more favorable interaction between CO₂ and the nanofluid.

3.3.3 Impact of SiO₂ NPs on CO₂/Nanofluid IFT at Supercritical Condition

The interfacial tension (IFT) between carbon dioxide (CO₂) and a nanofluid can be affected by variations in pressure and temperature, particularly in the context of supercritical conditions. Supercritical carbon dioxide (CO₂) denotes a phase where CO₂ exists at temperatures and pressures surpassing its critical point, manifesting characteristics resembling a gas and a liquid.

Introducing SiO₂ NPs into a CO₂/nanofluid can potentially result in diverse effects on the interfacial tension (IFT) between CO₂ and the nanofluid under supercritical conditions. This study evaluated interfacial tension (IFT) frequently by considering the influence of pressure and temperature. The results suggest a decrease in the value of γ at a concentration of 0.1 wt.% of SiO₂ NPs as the pressure was increased. The results are depicted in Fig. 24. To provide an example, the increase in pressure from 1100 to 1250 psi led to a decrease in the value of γ from 0.059948718 to 0.056321 mN/m (at a temperature of 32 °C and a concentration of 0.1 wt.% of SiO₂ NPs). Similarly, at a temperature of 35 °C and a concentration of 0.1 wt.% of SiO₂ NPs, the value of γ decreased from 0.054416667 to 0.053542 mN/m. The incorporation of SiO₂ NPs has resulted in reduced interfacial tension (IFT) between carbon dioxide and the nanofluid.



Fig. 22 Impact of pressure on IFT at constant temperature (40 °C)

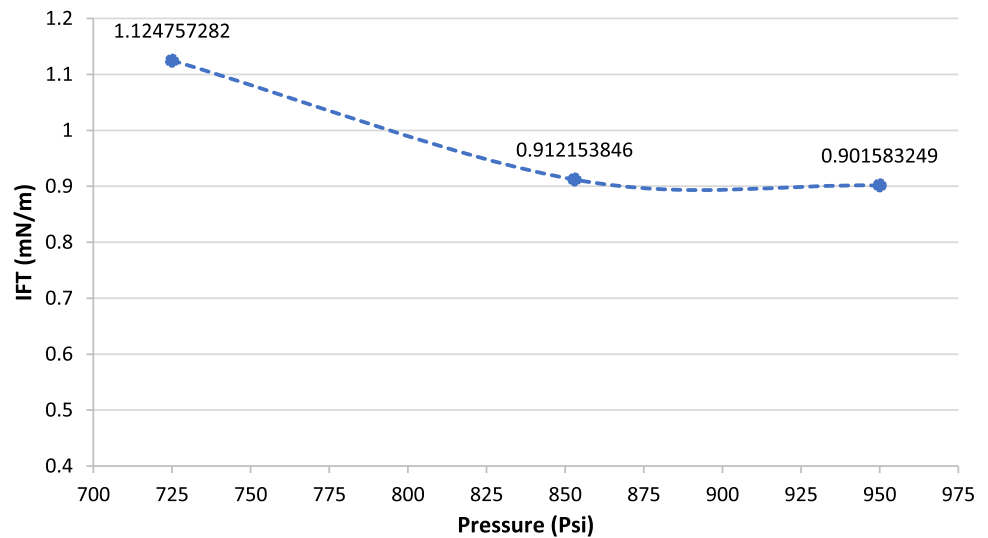


Fig. 23 Impact of temperature on IFT at constant pressure (at 853 psi)

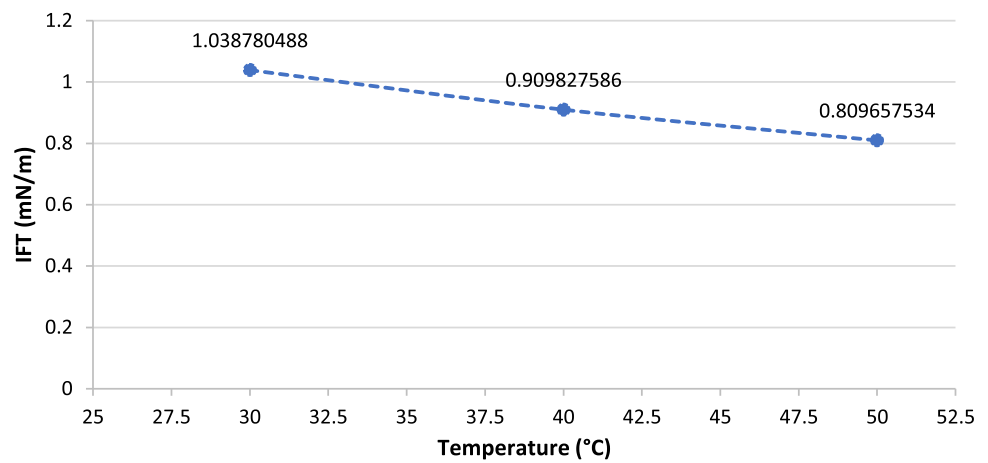


Fig. 24 Impact of SiO₂ NPs on CO₂/nanofluid IFT at supercritical conditions

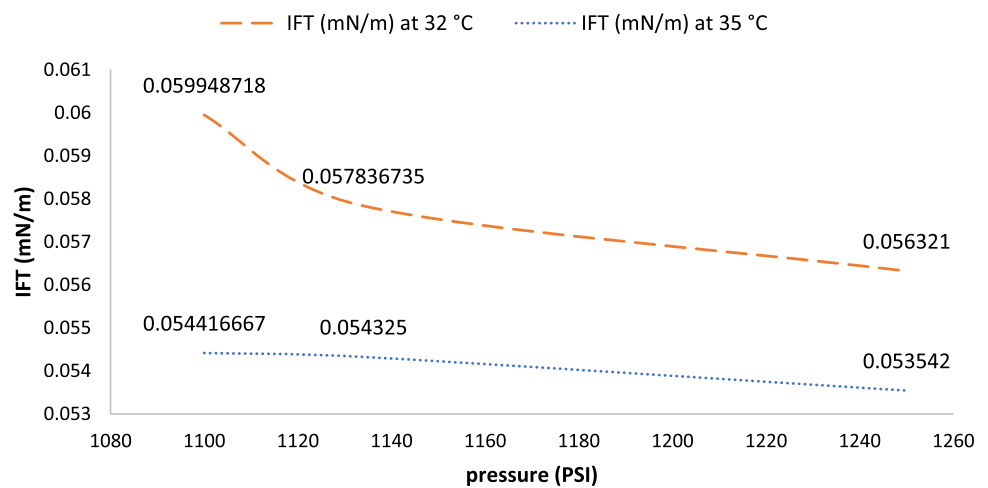
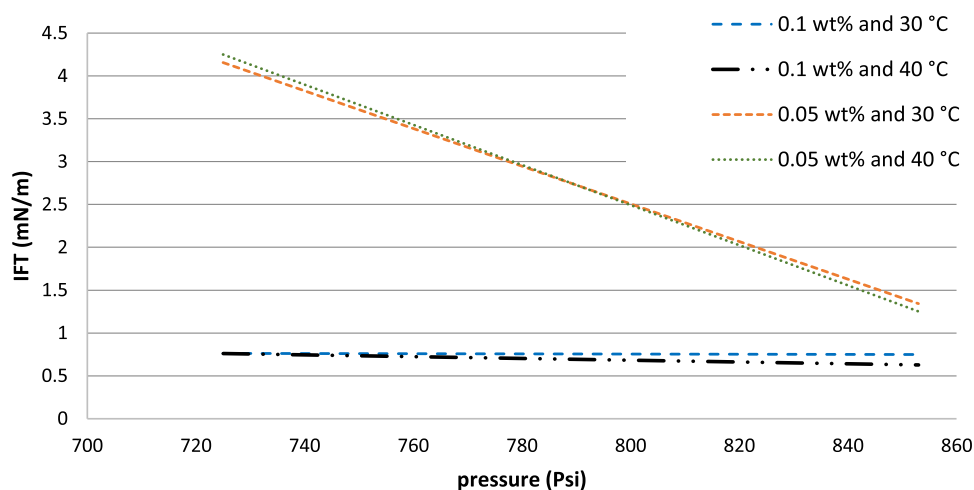


Fig. 25 Effect of pressure, temperature, and SiO₂/Xanthan NCs on the IFT measurements



Higher pressure reduced the interfacial tension (IFT) between carbon dioxide (CO₂) and the nanofluid. At elevated pressures, the density of supercritical CO₂ exhibits an augmentation, leading to an increased molecular packing density at the interface. The enhanced packing density decreases the interfacial tension (IFT) between carbon dioxide (CO₂) and the nanofluid. The extent of the pressure impact may differ based on the distinct characteristics of the nanofluid, encompassing the composition, concentration, and dimensions of NPs within it. The influence of temperature on the interfacial tension (IFT) of CO₂/nanofluid systems under supercritical conditions is also noteworthy. In general, it can be observed that there is a decrease in interfacial tension (IFT) as the temperature rises from 32 to 35 °C. Elevated temperatures augment the thermal energy within the system, thereby leading to heightened molecular motion and a decrease in the attractive forces between carbon dioxide (CO₂) and the nanofluid. Consequently, the IFT experiences a decrease.

The inclusion of NPs within the nanofluid has the potential to induce additional modifications to the interfacial tension (IFT) characteristics. The NPs can adsorb at the interface between CO₂ and nanofluid, forming a protective layer that effectively reduces the interfacial tension (IFT). The effectiveness of adsorption and subsequent reduction in interfacial tension can be influenced by nanoparticle size, concentration, and surface properties.

It is crucial to acknowledge that the influence of pressure and temperature on the interfacial tension (IFT) of CO₂/nanofluids under supercritical conditions can differ based on the nanofluid's composition and properties and the specific pressure and temperature parameters. Experimental investigations and thermodynamic modeling are frequently utilized to examine and forecast the behaviors of these systems.

3.3.4 Impact of SiO₂/Xanthan NCs on CO₂/Nanofluid IFT Measurements

Incorporating SiO₂/Xanthan nanocomposites into a CO₂/nanofluid can potentially impact the interfacial tension (IFT) between the CO₂ and the nanofluid. Here, interfacial tension (IFT) was often evaluated as a function of nanocomposite concentration, pressure, and temperature. The findings indicate that the value of γ declined as the concentration of NCs increased compared to CO₂-brine. The outcomes are presented in Fig. 25 and Table 6. As an illustration, the augmentation of NCs load from 0.05 to 0.1 wt.% resulted in a decline of γ from 4.157353 mN/m to 0.760282 at 725 Psi (at 30 °C), and from 1.2525 to 0.627349 mN/m at 853 Psi (at 40 °C). It has been discovered that adding SiO₂/Xanthan nanocomposites can decrease interfacial tension (IFT) between carbon dioxide and the nanofluid.

The phenomenon above can be attributed to the shuttle effect mechanism, whereby the NPs have the propensity to amass at the interface, leading to a consequential reduction in the interfacial area. Furthermore, increased pressure reduces interfacial tension (IFT) between carbon dioxide (CO₂) and a nanofluid. The phenomenon mentioned above can be attributed to the increase in pressure, which causes the compression of CO₂ and nanofluid phases. This compression can result in a decline in interfacial area and a corresponding reduction in interfacial tension.

The extent of reduction in interfacial tension (IFT) is commonly influenced by silicon dioxide (SiO₂) nanoparticle concentration. Typically, elevated concentrations of NPs result in a more significant reduction of interfacial tension (IFT). Nevertheless, NPs aggregate and coalesce into larger structures when present in exceedingly high concentrations, potentially augmenting the interfacial tension. However, the interfacial tension (IFT) between carbon dioxide (CO₂) and

Table 6 Calculated IFT of carbon dioxide-(SiO₂/Xanthan NCs) nanofluid by pendant drop methods

Exp#	nanomaterials type	Concentration wt.%	Pressure Psi	Temperature °C	Average IFT value mN/m
1	NCs-CO ₂	0.05 wt.% NCs	725	30	4.249333333
2	NCs-CO ₂	0.05 wt.% NCs	725	40	4.157352941
3	NCs-CO ₂	0.05 wt.% NCs	853	40	1.1625
4	NCs-CO ₂	0.05 wt.% NCs	853	30	1.341111111
5	NCs-CO ₂	0.1 wt.% NCs	853	40	0.627349398
6	NCs-CO ₂	0.1 wt.% NCs	853	30	0.75027972
7	NCs-CO ₂	0.1wt.% + 10wt.% NaCl	725	40	1.7125
8	NCs-CO ₂	0.1 wt.% + 5 wt.% NaCl	725	40	1.035178571
9	NCs-CO ₂	0.1 wt.% + 20 wt.% NaCl	725	40	4.564074074
10	NCs-CO ₂	0.1 wt.% NCs	725	30	0.72028169
11	NCs-CO ₂	0.1 wt.% NCs	725	40	0.759111111

a nanofluid exhibited a noteworthy augmentation as the temperature escalated from 30 to 40 °C, while maintaining a constant pressure of 725 Psi, as illustrated in Fig. 25.

Both silicon dioxide NPs (SiO₂ NPs) and silicon dioxide/xanthan nanocomposites (SiO₂/ xanthan NCs) exhibited a significant reduction in interfacial tension (IFT) when compared to CO₂-brine, as presented in Table 6. Furthermore, it can be observed that the degree of IFT alteration in SiO₂ NPs is more pronounced when compared to SiO₂/Xanthan nanocomposite systems under conditions of increasing concentration, pressure, and temperature. Recent studies have indicated that elevating pressure can exert a more pronounced impact on interfacial tension (IFT) in nanofluids characterized by reduced particle sizes or augmented nanoparticle densities. Furthermore, it has been observed that the pressure sensitivity of interfacial tension (IFT) measurements can be influenced by temperature, whereby certain nanofluids demonstrate heightened pressure sensitivity at elevated temperatures.

In terms of temperature, the effect on IFT measurements in CO₂/nanofluid systems can vary. Increasing the temperature from 30 to 40 °C for all pressure conditions and SiO₂/Xanthan nanocomposite concentration decreases the IFT. This reduction in IFT can be attributed to the increased thermal energy, which facilitates the mobility and rearrangement of molecules at the interface, leading to a more favorable interaction between CO₂ and the nanofluid.

3.3.5 Effect of Salt Concentration on CO₂/Nanofluid IFT Measurements

The effect of NaCl salt concentration on CO₂/nanofluid (i.e., SiO₂/Xanthan NCs) interfacial tension (IFT) measurements

can depend on several factors, including the concentration and type of NPs in the nanofluid, the pressure, the temperature, and the interaction between the salt and the NPs. In this study, we want to investigate the effect of NaCl salt concentration on CO₂/nanofluid IFT, as the NaCl concentration increased from 5 to 20 wt.% significantly increased the interfacial tension between CO₂ and a nanofluid from 1.0352 to 4.564 mN/m because it is difficult to achieve effective CO₂/nanofluid mixing and promote the formation of CO₂ bubbles. The degree of this effect may be influenced by the NaCl concentration, as depicted in Fig. 26.

One mechanism by which NaCl salt increases IFT is through the formation of an ion-pairing effect at the interface between CO₂ and the nanofluid. Increasing IFT can lead to the adsorption of Na⁺ and Cl⁻ ions at the interface and the formation of a salt layer. Overall, the effect of NaCl salt concentration on CO₂/nanofluid IFT measurements is complex and can depend on various factors. Understanding this relationship is important for designing and optimizing CO₂/nanofluid processes for CO₂ sequestration in brine formation.

4 Correlation Between the CO₂/Nanofluid IFT with Diffusion Coefficient in the Context of CO₂ Sequestration

The correlation between the interfacial tension (IFT) of carbon dioxide (CO₂) and a nanofluid was established based on the diffusion coefficient of CO₂ within the nanofluid. The diffusion coefficient signifies the rate at which CO₂ molecules move or diffuse through the nanofluid. This diffusion rate was subject to modification by various factors, including the

Fig. 26 CO₂/nanofluid (0.01 wt. % NCs) IFT value as a function of the NaCl salt concentration at pressure 853 Psi and temperature 40 °C

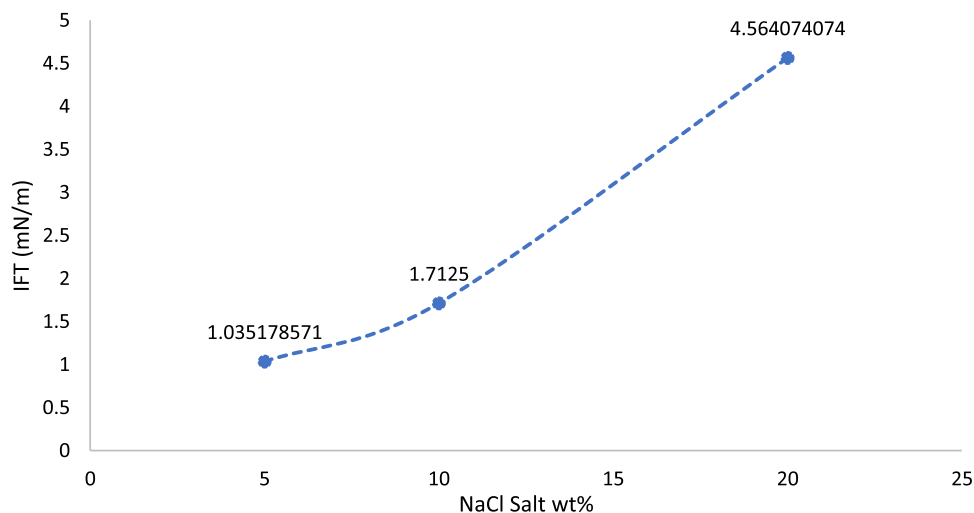
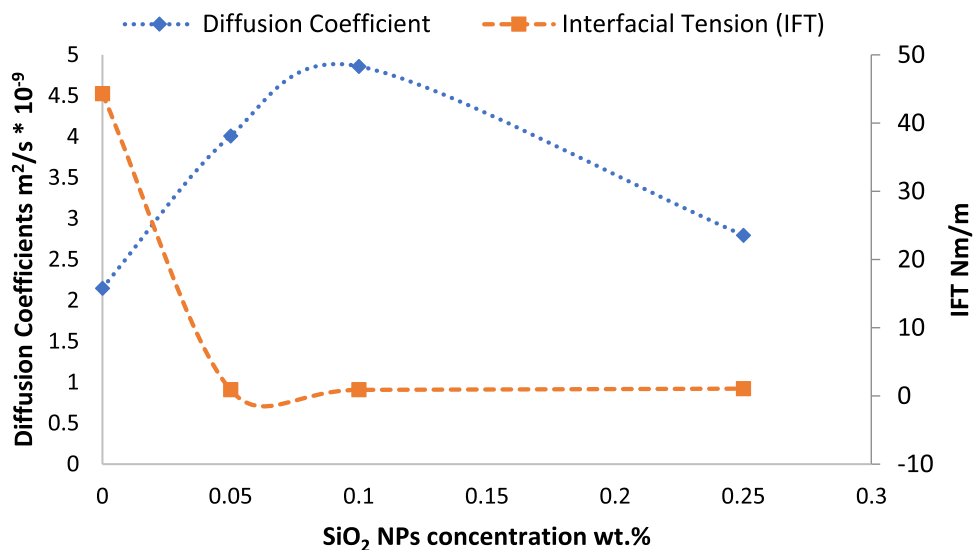


Fig. 27 Correlation between the CO₂/nanofluid IFT with diffusion coefficient at different NPs concentration



concentration, pressure, temperature, as well as the size and shape of nanoparticles (NPs) present in the nanofluid.

In many instances during our experiments, there was an observed inverse relationship between the CO₂ diffusion coefficient and IFT, as demonstrated in Figs. 27 and 28. In Fig. 27, when the nanofluid contained 0.1 wt. % SiO₂ NPs compared to that without NPS, the IFT decreased from 44.35 to 0.91 Nm/m. Simultaneously, the CO₂ diffusion coefficient increased from 2.149×10^{-9} to 4.86×10^{-9} m²/s.

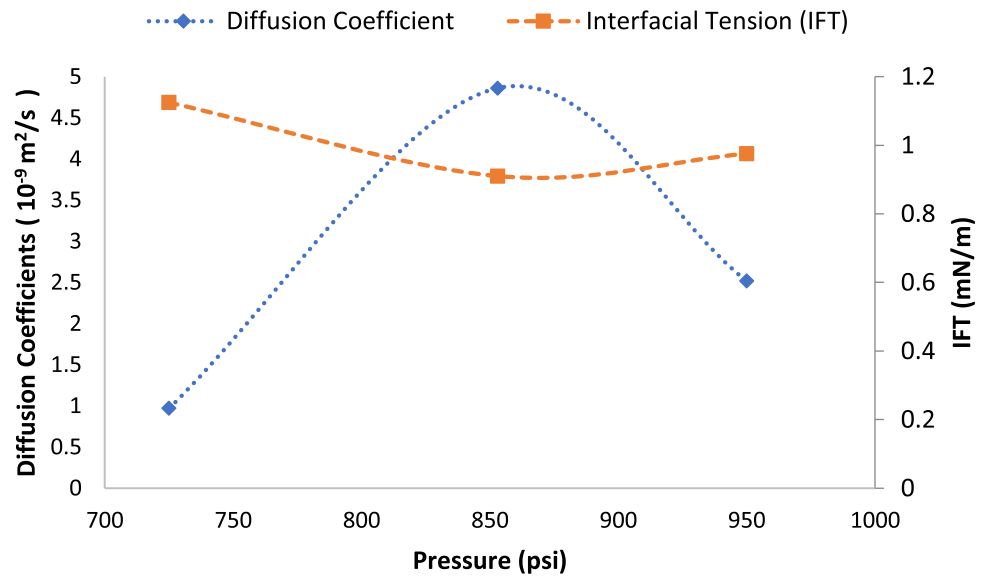
Additionally, in Fig. 28, at a constant NPs concentration, increasing pressure or temperature led to a decrease in IFT, while the diffusion coefficient consistently increased, indicating more efficient CO₂ transport through the nanofluid.

The possible correlation between CO₂ diffusion and IFT can be attributed to the shuttle effect. In this effect, the NPs

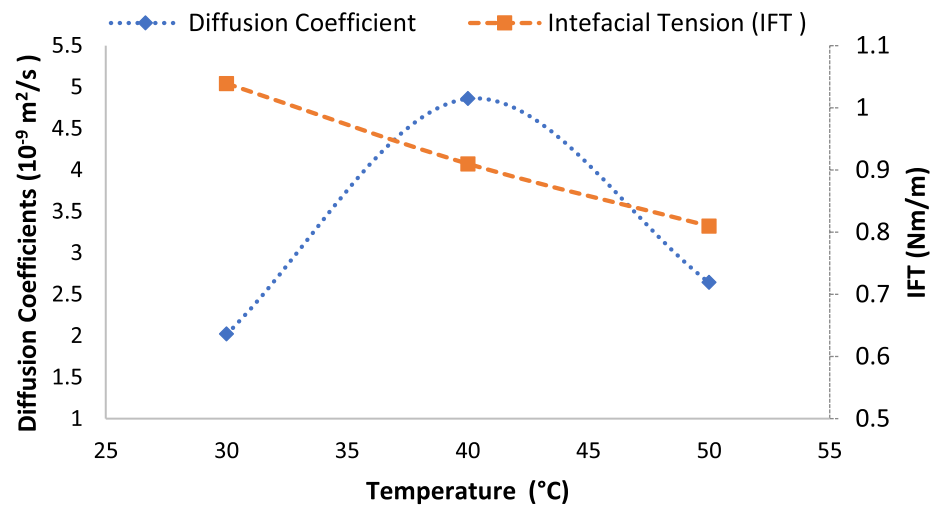
within the nanofluid act as shuttles that both facilitate and hinder CO₂ transportation across the interface separating CO₂ and the nanofluid. This phenomenon results in decreased IFT and an enhancement in CO₂ dissolution within the nanofluid. An increase in the diffusion coefficient of CO₂ in the nanofluid reduces the IFT between CO₂ and the nanofluid. The rationale behind this is that an increased diffusion facilitates the movement of CO₂ molecules through the nanofluid, thereby enhancing the shuttle effect and reducing the interfacial tension.

These findings provide valuable insights into the behavior of CO₂ within nanofluids and have implications for optimizing carbon capture and storage processes, with the potential to contribute to more efficient and sustainable strategies for addressing greenhouse gas emissions and climate change.

Fig. 28 Correlation between the CO₂/nanofluid IFT with diffusion coefficient, **a** pressure changes, **b** temperature difference



(a)



(b)

5 Conclusion

The use of green nanomaterials in CO₂ sequestration has gained interest due to their potential to reduce the environmental impact of the sequestration process. This study first investigated the effect of green SiO₂ NPs (NPs) and SiO₂/Xanthan NCs on the CO₂/nanofluid system’s diffusion coefficient. This was done using the pressure decay “Sheikha method,” which was then applied in a high-precision Fluid EVAL PVT cell under saline CO₂ sequestration conditions (high pressure and high temperature). This is followed by experimental methods to determine the interfacial tension (IFT) of CO₂/nanofluid using the Pendant drop method. The

measured data for the CO₂-brine/nanofluid system were consistent regarding the effect of concentration, pressure, temperature, phase alteration, and salinity. The present study draws the following conclusions:

- (i) The experimental findings reveal that the most favorable CO₂ diffusion coefficient was achieved within the tested ranges of nanoparticle (NPS) concentration, pressure, and temperature, specifically at 0.1 wt.% concentration, 850 Psi pressure, and a temperature of 40 °C. These conditions represent the optimal combination for the observed CO₂ diffusion coefficient in our study.

- (ii) The experimental results show that the CO₂ diffusion coefficient increases with nanofluid concentration and pressure rises. At the same time, the CO₂/nanofluid IFT decreases with both nanoparticle concentration and pressure increase.
- (iii) Generally, an increase in temperature at constant pressure led to a decrease in the interfacial tension (IFT) between CO₂ and the nanofluid, while it resulted in an increase in the CO₂ diffusion coefficient.
- (iv) The diffusion coefficient became independent of changes in pressure or temperature when temperature or pressure exceeded a critical point (about T_c and P_c of CO₂).
- (v) The obtained results showed SiO₂ NPS and SiO₂/Xanthan NCs enhanced the CO₂ diffusion coefficient in nanofluids due to their large surface area and high adsorption capacity for CO₂. It has also been shown to reduce the nano-CO₂ IFT by forming a stable interfacial layer, which can enhance the dissolution of CO₂ in the nanofluid.
- (vi) SiO₂ NPs exhibit Brownian motion due to thermal fluctuations, which enhances the diffusion of CO₂ in the nanofluid.
- (vii) SiO₂ NPs induced the shuttle effect, which involves the transfer of CO₂ molecules from one nanoparticle to another. This can enhance the IFT of CO₂/nanofluid and improve the CO₂ diffusion.

Using NPs in CO₂/nanofluids can improve CO₂ diffusion coefficients and reduce interfacial tension with brine formations by combining Brownian motion, adsorption, nanoparticle size and concentration, and the Shuttle effect. These mechanisms can lead to more efficient CO₂ sequestration in brine formations.

References

1. Heidari, N.; Pearce, J.M.: A review of greenhouse gas emission liabilities as the value of renewable energy for mitigating lawsuits for climate change related damages. *Renew. Sustain. Energy Rev.* **55**, 899–908 (2016). <https://doi.org/10.1016/j.rser.2015.11.025>
2. Yoro, K.O.; Daramola, M.O.: CO₂ emission sources, greenhouse gases, and the global warming effect. In: *Advances in Carbon Capture: Methods, Technologies and Applications*, pp. 3–28. Elsevier, Amsterdam (2020). <https://doi.org/10.1016/B978-0-12-819657-1.00001-3>
3. Wu, P.; Xia, B.; Zhao, X.: The importance of use and end-of-life phases to the life cycle greenhouse gas (GHG) emissions of concrete—a review. *Renew. Sustain. Energy Rev.* **37**, 360–369 (2014). <https://doi.org/10.1016/j.rser.2014.04.070>
4. Sovacool, B.K.; Brown, M.A.: Twelve metropolitan carbon footprints: a preliminary comparative global assessment. *Energy Policy* **38**, 4856–4869 (2010). <https://doi.org/10.1016/j.enpol.2009.10.001>
5. Caiazzo, F.; Ashok, A.; Waitz, I.A.; Yim, S.H.L.; Barrett, S.R.H.: Air pollution and early deaths in the United States Part I: quantifying the impact of major sectors in 2005. *Atmos. Environ.* **79**, 198–208 (2013). <https://doi.org/10.1016/j.atmosenv.2013.05.081>
6. Aresta, M.; Dibenedetto, A.; Angelini, A.: The changing paradigm in CO₂ utilization. *J. CO₂ Util.* **3–4**, 65–73 (2013). <https://doi.org/10.1016/j.jcou.2013.08.001>
7. Chu, S.; Majumdar, A.: Opportunities and challenges for a sustainable energy future. *Nature* **488**, 294–303 (2012). <https://doi.org/10.1038/nature11475>
8. Ali, M.; Jha, N.K.; Pal, N.; Keshavarz, A.; Hoteit, H.; Sarmadivaleh, M.: Recent advances in carbon dioxide geological storage, experimental procedures, influencing parameters, and future outlook. *Earth Sci. Rev.* **225**, 103895 (2022). <https://doi.org/10.1016/j.earscirev.2021.103895>
9. Raza, A.; Gholami, R.; Rezaee, R.; Rasouli, V.; Rabiei, M.: Significant aspects of carbon capture and storage—a review. *Petroleum* **5**, 335–340 (2019). <https://doi.org/10.1016/j.petlm.2018.12.007>
10. Stewart, C.; Hessami, M.A.: A study of methods of carbon dioxide capture and sequestration—the sustainability of a photosynthetic bioreactor approach. *Energy Convers. Manag.* **46**, 403–420 (2005). <https://doi.org/10.1016/j.enconman.2004.03.009>
11. Holloway, S.: Underground sequestration of carbon dioxide—a viable greenhouse gas mitigation option. *Energy* **30**, 2318–2333 (2005). <https://doi.org/10.1016/j.energy.2003.10.023>
12. Leung, D.Y.C.; Caramanna, G.; Maroto-Valer, M.M.: An overview of current status of carbon dioxide capture and storage technologies. *Renew. Sustain. Energy Rev.* **39**, 426–443 (2014). <https://doi.org/10.1016/j.rser.2014.07.093>
13. Jafari Raad, S.M.; Azin, R.; Osfouri, S.: Measurement of CO₂ diffusion in synthetic and saline aquifer solutions at reservoir conditions: the role of ion interactions. *Heat Mass Transf.* **51**, 1587–1595 (2015)
14. Gershenzon, N.I.; Ritzi, R.W.; Dominic, D.F.; Mehnert, E.: Effective constitutive relations for simulating CO₂ capillary trapping in heterogeneous reservoirs with fluvial sedimentary architecture. *Geomech. Geophys. Geo-Energy Geo-Resour.* **3**, 265–279 (2017). <https://doi.org/10.1007/s40948-017-0057-3>
15. Gschwend, P.M.: Enhanced concentrations of PAHs in groundwater at a coal tar site. *Environ. Sci. Technol.* **35**, 1320–1328 (2001)
16. Subba-Rao, V.; Hoffmann, P.M.; Mukhopadhyay, A.: Tracer diffusion in nanofluids measured by fluorescence correlation spectroscopy. *J. Nanopart. Res.* **13**, 6313–6319 (2011). <https://doi.org/10.1007/s11051-011-0607-5>
17. Yu, W.; Xie, H.: A review on nanofluids: preparation, stability mechanisms, and applications. *J. Nanomater.* **1–17**, 2012 (2012). <https://doi.org/10.1155/2012/435873>
18. Rezk, M.G.; Foroozesh, J.; Abdulrahman, A.; Gholinezhad, J.: CO₂ diffusion and dispersion in porous media: review of advances in experimental measurements and mathematical models. *Energy Fuels* **36**(1), 133–155 (2021)
19. Sigmund P.M.; Sigmund P.M.: Prediction of molecular diffusion at reservoir conditions. Part I measurement and prediction of binary dense gas diffusion coefficients. n.d
20. Riazi, M.R.; Whitson, C.H.; Da Silva, F.: Modelling of diffusional mass transfer in naturally fractured reservoirs. *J. Petrol. Sci. Eng.* **10**, 239–253 (1994)
21. Reza Etmiman, S.; Pooladi-Darvish, M.; Maini, B.B.; Chen, Z.: Modeling the interface resistance in low soluble gaseous solvents-heavy oil systems. *Fuel* **105**, 672–687 (2013). <https://doi.org/10.1016/j.fuel.2012.08.048>
22. Grogan, A.T.; Pinczewski, V.W.; Ruskauff, G.J.; Orr, F.: Diffusion of CO₂ at reservoir conditions: models and measurements. *SPE Reserv. Eng.* **3**, 93–102 (1988)
23. Lu, W.; Guo, H.; Chou, I.M.; Burruss, R.C.; Li, L.: Determination of diffusion coefficients of carbon dioxide in water between



- 268 and 473K in a high-pressure capillary optical cell with in situ Raman spectroscopic measurements. *Geochim. Cosmochim. Acta* **115**, 183–204 (2013). <https://doi.org/10.1016/j.gca.2013.04.010>
24. Li, S.; Qiao, C.; Zhang, C.; Li, Z.: Determination of diffusion coefficients of supercritical CO₂ under tight oil reservoir conditions with pressure-decay method. *J. CO₂ Util.* **24**, 430–443 (2018). <https://doi.org/10.1016/j.jcou.2018.02.002>
 25. Lv, J.; Chi, Y.; Zhao, C.; Zhang, Y.; Mu, H.: Experimental study of the supercritical CO₂ diffusion coefficient in porous media under reservoir conditions. *R Soc. Open Sci.* **6**, 181902 (2019). <https://doi.org/10.1098/rsos.181902>
 26. Shu, G.; Dong, M.; Hassanzadeh, H.; Chen, S.: Effects of operational parameters on diffusion coefficients of CO₂ in a carbonated water-oil system. *Ind. Eng. Chem. Res.* **56**, 12799–12810 (2017). <https://doi.org/10.1021/acs.iecr.7b02546>
 27. Policarpo, N.A.; Ribeiro, P.R.: Experimental measurement of gas-liquid diffusion. *Braz. J. Petrol. Gas* **5**, 171–188 (2011). <https://doi.org/10.5419/bjjpg2011-0017>
 28. Zhang, Z.; Cai, J.; Chen, F.; Li, H.; Zhang, W.; Qi, W.: Progress in enhancement of CO₂ absorption by nanofluids: a mini review of mechanisms and current status. *Renew. Energy* **118**, 527–535 (2018). <https://doi.org/10.1016/j.renene.2017.11.031>
 29. Kim, S.; Tserengombo, B.; Choi, S.H.; Noh, J.; Huh, S.; Choi, B., et al.: Experimental investigation of heat transfer coefficient with Al₂O₃ nanofluid in small diameter tubes. *Appl. Therm. Eng.* **146**, 346–355 (2019). <https://doi.org/10.1016/j.applthermaeng.2018.10.001>
 30. Krishnamurthy, S.; Bhattacharya, P.; Phelan, P.E.; Prasher, R.S.: Enhanced mass transport in nanofluids. *Nano Lett.* **6**, 419–423 (2006). <https://doi.org/10.1021/nl052253z>
 31. Farzani Tolesorkhi, S.; Esmailzadeh, F.; Riazi, M.: Experimental and theoretical investigation of CO₂ mass transfer enhancement of silica nanoparticles in water. *Petrol. Res.* **3**, 370–380 (2018). <https://doi.org/10.1016/j.ptlrs.2018.09.002>
 32. Rashidi, H.; Mamivand, S.: Experimental and numerical mass transfer study of carbon dioxide absorption using Al₂O₃/water nanofluid in wetted wall column. *Energy* **238**, 121670 (2022). <https://doi.org/10.1016/j.energy.2021.121670>
 33. Youns, Y.T.; Manshad, A.K.; Ali, J.A.: Sustainable aspects behind the application of nanotechnology in CO₂ sequestration. *Fuel* **349**, 128680 (2023). <https://doi.org/10.1016/j.fuel.2023.128680>
 34. Al-Anssari, S.; Barifcani, A.; Keshavarz, A.; Iglauer, S.: Impact of nanoparticles on the CO₂-brine interfacial tension at high pressure and temperature. *J. Colloid Interface Sci.* **532**, 136–142 (2018). <https://doi.org/10.1016/j.jcis.2018.07.115>
 35. Arbabpour Jannatabadi, A.; Bastani, D.; Norouzbahari, S.; Ghadimi, A.: CO₂ and CH₄ diffusivities through synthesized ZIF-8 nanocrystals: an experimental and theoretical investigation. *Micro-porous Mesoporous Mater.* **324**, 111292 (2021). <https://doi.org/10.1016/j.micromeso.2021.111292>
 36. Sharafi, M.S.; Ghasemi, M.; Ahmadi, M.; Kazemi, A.: An experimental approach for measuring carbon dioxide diffusion coefficient in water and oil under supercritical conditions. *Chin. J. Chem. Eng.* **34**, 160–170 (2021). <https://doi.org/10.1016/j.cjche.2020.08.034>
 37. Zhou, B.; Li, Q.; Zhang, Q.; Duan, J.; Jin, W.: Sharply promoted CO₂ diffusion in a mixed matrix membrane with hierarchical supra-nanostructured porous coordination polymer filler. *J. Memb. Sci.* **597**, 117772 (2020). <https://doi.org/10.1016/j.memsci.2019.117772>
 38. Guo, A.; Ban, Y.; Yang, K.; Yang, W.: Metal-organic framework-based mixed matrix membranes: synergetic effect of adsorption and diffusion for CO₂/CH₄ separation. *J. Memb. Sci.* **562**, 76–84 (2018). <https://doi.org/10.1016/j.memsci.2018.05.032>
 39. Dehghan, P.; Azari, A.; Azin, R.: Measurement and correlation for CO₂ mass diffusion in various metal oxide nanofluids. *J. Environ. Chem. Eng.* **8**(1), 103598 (2020)
 40. Chen, J.; Liu, T.; Zhao, L.; Yuan, W.K.: Experimental measurements and modeling of solubility and diffusion of CO₂ in polypropylene/micro-and nanocalcium carbonate composites. *Ind. Eng. Chem. Res.* **52**, 5100–5110 (2013). <https://doi.org/10.1021/ie303587r>
 41. Nazarahari, M.J.; Manshad, A.K.; Ali, M.; Ali, J.A.; Shafiei, A.; Sajadi, S.M., et al.: Impact of a novel biosynthesized nanocomposite (SiO₂@Montmorillonite@Xanthan) on wettability shift and interfacial tension: applications for enhanced oil recovery. *Fuel* **298**, 120773 (2021). <https://doi.org/10.1016/j.fuel.2021.120773>
 42. Sheikha, H.; Pooladi-Darvish, M.; Mehrotra, A.K.: Development of graphical methods for estimating the diffusion coefficient of gases in bitumen from pressure-decay data. *Energy Fuels* **19**, 2041–2049 (2005). <https://doi.org/10.1021/ef050057c>
 43. Thakur, S.; Pandey, S.; Arotiba, O.A.: Sol-gel derived xanthan gum/silica nanocomposite—a highly efficient cationic dyes adsorbent in aqueous system. *Int. J. Biol. Macromol.* **103**, 596–604 (2017). <https://doi.org/10.1016/j.ijbiomac.2017.05.087>
 44. Dubey, R.S.; Rajesh, Y.B.R.D.; More, M.A.: Synthesis and characterization of SiO₂ nanoparticles via Sol-gel method for industrial applications. *Mater. Today Proc.* **2**, 3575–3579 (2015). <https://doi.org/10.1016/j.matpr.2015.07.098>
 45. Do, H.D.: Diffusion controlled swelling of reservoir oil by direct contact with injection gas. *Chem. Eng. Sci.* **46**, 1259–1270 (1991)
 46. Sarmadivaleh, M.; Al-Yaseri, A.Z.; Iglauer, S.: Influence of temperature and pressure on quartz-water-CO₂ contact angle and CO₂-water interfacial tension. *J. Colloid Interface Sci.* **441**, 59–64 (2015). <https://doi.org/10.1016/j.jcis.2014.11.010>
 47. Arif, M.; Al-Yaseri, A.Z.; Barifcani, A.; Lebedev, M.; Iglauer, S.: Impact of pressure and temperature on CO₂-brine-mica contact angles and CO₂-brine interfacial tension: Implications for carbon geo-sequestration. *J. Colloid Interface Sci.* **462**, 208–215 (2016). <https://doi.org/10.1016/j.jcis.2015.09.076>
 48. Georgiadis, A.; Maitland, G.; Trusler, J.P.M.; Bismarck, A.: Interfacial tension measurements of the (H₂O + n-decane + CO₂) ternary system at elevated pressures and temperatures. *J. Chem. Eng. Data* **56**, 4900–4908 (2011). <https://doi.org/10.1021/je200825j>
 49. Jha, N.K.; Ivanova, A.; Lebedev, M.; Barifcani, A.; Cheremisin, A.; Iglauer, S., et al.: Interaction of low salinity surfactant nanofluids with carbonate surfaces and molecular level dynamics at fluid-fluid interface at ScCO₂ loading. *J. Colloid Interface Sci.* **586**, 315–325 (2021). <https://doi.org/10.1016/j.jcis.2020.10.095>

Springer Nature or its licensor (e.g. a society or other partner) holds exclusive rights to this article under a publishing agreement with the author(s) or other rightsholder(s); author self-archiving of the accepted manuscript version of this article is solely governed by the terms of such publishing agreement and applicable law.

